Experimental phase-equilibrium study of Al- and Ti-contents of calcic amphibole in MORB—A semiquantitative thermobarometer

W.G. Ernst* and Jun Liu

Department of Geological and Environmental Sciences, Stanford University, Stanford, California 94305-2115, U.S.A.

Abstract

Calcic amphiboles were synthesized from a natural mid-ocean ridge basalt (MORB) in 39 experiments representing 24 sets of pressure-temperature (*P-T*) conditions ranging from 650–950 °C, 0.8–2.2 GPa, at f_{O_2} controlled by the fayalite-magnetite-quartz (FMQ) buffer, and $P_{aqueous\ fluid} = P_{total}$. Experiments lasted up to 1630 h at low temperatures; in all cases, synthesized hornblendes were coarse-grained ($5–7 \times 10–15$ μm) and chemically homogeneous. Over the investigated pressure range, Ca-amphibole coexisting with phases rich in Al and Ti gradually changes composition from sodic-calcic, Si-rich at low temperatures to calcic, Si-poor at high temperatures: it is barroisite at 650 °C, edenite at 700 °C, and pargasite at 800–950 °C. Electron microprobe data were combined with 41 comparable analyses from the literature for Ca-amphiboles synthesized from MORBs at intermediate f_{O_2} in order to erect a petrogenetic grid for the experimental range 0.0–2.2 GPa, 450–1050 °C. Isopleths for Al_2O_3 in Ca-amphibole exhibit markedly negative *P-T* slopes, indicating increasing Al_2O_3 contents with both *P* and *T*. In contrast, TiO_2 isopleths are nearly independent of *P*, demonstrating that TiO_2 in Ca-amphibole increases almost exclusively as a function of *T*. For natural metabasaltic assemblages that contain coexisting Al-rich and Ti-rich phases, and closely approached chemical equilibrium under crustal or uppermost mantle conditions, this semiquantitative petrogenetic grid allows the simultaneous assignment of attendant *P* and *T* employing Ca-amphibole Al_2O_3 and TiO_2 contents. However, during slow cooling, natural Ca-amphiboles may exsolve TiO_2 as rutile, titanite, and/or ilmenite, but in general do not redistribute Al_2O_3, so this thermobarometer must be applied with caution to inhomogeneous specimens.

Introduction

Calcic amphibole-bearing metabasaltic rocks are an important and, in some cases, dominant lithology in metamorphosed portions of both continental and oceanic crust. Because of its volumetric importance and broad range of natural occurrences, information concerning the crystal-chemical behavior of Ca-amphibole in metabasaltic rocks as a function of the attending conditions of recrystallization is critical for the determination of the state variables *P* and *T*. Numerous studies have dealt with parageneses of Ca-amphiboles in mafic igneous rocks (e.g., Shido and Miyashiro 1959; Engel and Engel 1962; Deer et al. 1963; Leake 1965; Ernst 1972a, 1979; Thompson 1981; Robinson et al. 1982; Wones and Gilbert 1982; Graham and Powell 1984; Blundy and Holland 1990; Holland and Blundy 1994). These studies make it clear that, with increasing metamorphic grade, Ca-amphiboles exhibit increases in Mg/(Mg+Fe), and Ti, Al, Na, and K contents, and commensurate decreases in Si and total Fe+Mg+Mn±Ca. These changes reflect increases in the tschermakitic, pargasitic, and edenitic substitutions as a consequence of net-transfer reactions as well as exchange equilibria. Serious difficulties in relating Ca-amphibole chemistry to the conditions of metamorphism reflect the fact that its crystal structure includes several rather compliant cation sites, capable of accommodating elements having a wide range of ionic radii and valences. Moreover, in many metabasalts, associated neoblastic phases are few, thus the buffering capacity of low-variance assemblages is not commonly realized. Accordingly, Ca-amphiboles, which contain 6–10 essential components (Leake 1978), in general mirror the bulk-rock composition of the parental metabasalt itself.

Because mafic igneous rocks are nearly ubiquitous in crustal terranes, and are relatively uniform in bulk composition, experiments on MORBs under controlled laboratory conditions (*P, T,* f_{O_2}) have the capability of yielding important constraints on the metamorphic stability relations of this rock type, including the chemical variability of constituent Ca-amphiboles. Unfortunately, virtually all experimental attempts to demonstrate equilibrium by reaction reversal remain equivocal, reflecting the complicated nature of gradational, multicomponent reactions with changing *P* and *T,* as well as the sluggish rates of recrystallization. Because of such difficulties, few such phase-synthesis studies actually have been carried out.

* E-mail: ernst@pangea.stanford.edu

TABLE 1. Chemical compositions (gravimetric analyses) of MORBs and experimental bulk compositions

Oxide	No. 1	No. 2	No. 3	This study	No. 4	No. 5	No. 6	No. 7	No. 8
SiO_2	50.68	50.93	50.19	50.10	49.7	50.44	49.43	52.38	49.11
Al_2O_3	15.60	15.15	14.86	14.80	12.8	13.37	15.97	16.93	12.74
Fe_2O_3	1.48	1.55	1.70	1.89	1.95	2.23	2.09	—	3.23
FeO	8.37	8.02	9.63	10.72	9.95	11.27	7.55	10.29*	8.40
MgO	7.69	7.69	7.10	7.00	9.04	6.58	8.50	7.13	10.31
MnO	—	—	—	0.22		0.21	0.18	—	0.17
TiO_2	1.49	1.19	1.77	1.25	1.54	1.79	1.62	—	2.51
CaO	11.44	11.84	11.44	11.10	10.9	10.95	10.73	10.05	10.73
Na_2O	2.66	2.32	2.66	2.57	1.93	3.76	2.87	3.21	1.97
K_2O	0.17	0.14	0.16	0.14	0.06	0.19	0.18	—	0.49
P_2O_5	0.12	0.10	0.14	—		0.20	0.15	—	0.27
Total	99.70	98.93	99.65	99.79	99.28	100.75	99.27	99.99	99.93
CIPW normative minerals									
Quartz		1.1			1.0				
Orthoclase	1.0	0.8	1.0	0.8	0.4	1.1	1.1		2.9
Albite	22.6	19.8	22.6	21.8	16.7	31.5	26.0	27.2	16.7
Anorthite	30.2	30.8	28.2	28.5	26.7	18.9	30.2	31.8	24.7
Nepheline									
Diopside	21.1	22.7	22.8	22.0	23.3	27.8	17.8	14.9	22.0
Hypersthene	17.6	19.9	17.4	18.0	26.1		13.4	20.1	19.8
Olivine	2.2		1.9	3.8		13.7	6.1	4.0	7.3
Magnetite	2.2	2.3	2.5	2.8	2.9	3.2	2.2	2.2	1.2
Ilmenite	2.8	2.3	3.4	2.4	3.0	3.4	2.2		4.8
Apatite	0.3	0.2	0.3	0.0		0.4	0.3		0.6

Note: No. 1 = Mid-Atlantic Ridge (Melson et al. 1976); No. 2 = Indian Ocean Ridge (Melson et al. 1976); No. 3 = East Pacific Rise (Melson et al. 1976); No. 4 = Liou et al. (1974); No. 5 = Apted + Liou (1983); No. 6 = Spear (1981); No. 7 = Poli (1993); No. 8 = Helz (1979).
 * Total iron, XRF analysis.

Nonetheless, carefully controlled, long-duration experiments in some cases have produced Ca-amphiboles sufficiently large to obtain a high-quality electron microprobe analysis (EMPA), thus affording the opportunity to check for phase homogeniety, a necessary but insufficient condition of chemical equilibrium.

It is well known that Al tends to replace Si in tetrahedral coordination in Ca-amphibole with increasing T, whereas Al substitutes for Mg+Fe in the M2 octahedral site to progressively greater extents with increasing P (Raase 1974; Hawthorne 1981; Gilbert et al. 1982; Robinson et al. 1982; Anderson and Smith 1995). Accordingly, it seems likely that the Al_2O_3 content of Ca-amphibole increases as a function of both P and T (e.g., Moody et al. 1983). Titanium is also increasingly accommodated in the amphibole M2 site as temperature rises (Raase 1974), but this cation should be less favored by increasing P because of its relatively larger ionic radius compared with Al. For this reason, it seems probable that Ti concentration in Ca-amphibole will track positively with T, but perhaps slightly negatively with P. Thus, in rocks that contain a Ti-rich phase such as ilmenite, titanite, or rutile, and are therefore saturated in Ti—which, in addition, carry appropriate, highly aluminous phases such as plagioclase, epidote, or garnet—the isopleths for Al_2O_3 and TiO_2 in Ca-amphibole will display contrasting behavior. Ideally, for metabasalts of typical MORB-like chemistry, the P-T conditions of metamorphism should be obtainable, at least approximately, from analysis of the constituent Ca-amphibole, if we knew how Al and Ti vary with physical conditions. In the present paper, we explore this relationship quantitatively, and report a promising measure of success.

EXPERIMENTAL TECHNIQUES

Starting materials

We used natural basaltic glass and a crystal mixture synthesized from the glass as starting materials for all experiments. The glass, dredged from the Juan de Fuca Ridge off the coast of Oregon, is homogeneous and contains minor crystallites (<1%) of pyroxene, plagioclase, and ilmenite, judging from optical microscopy and electron microprobe backscattered electron (BSE) imagery. The chemical composition and CIPW norm of the glass as well as those of typical MORBs, some of which have been employed in other experimental phase equilibrium studies, are listed in Table 1. It is important to note that the norm calculation is sensitive to the Fe^{3+} content of the basalt: the glass used in our experiments is slightly olivine normative assuming $Fe^{3+}/Fe_T = 0.15$, but quartz normative assuming $Fe^{3+}/Fe_T = 0.25$.

The glass was crushed in a tungsten carbide ball mill and ground under ethanol in an agate mortar for 3 h, followed by drying in an oven at 130 °C for 24 h. Most experiments were not seeded with crystals. However, in order to overcome the difficulty of nucleation, for some experiments approaching phase boundaries, or at subsolidus temperatures, small amounts of seed (less than 0.5% by weight) of synthetic almandine-grossular garnet ($Alm_{80}Gro_{20}$), and/or natural lawsonite and clinozoisite, were added to the starting mixtures. The amounts of seed crystals added were small, so the bulk composition of the system remained essentially unchanged. The compositions of the garnet seeds were different from those of the synthesized products, hence they were readily identified using BSE imagery.

TABLE 2. EMPA Ca-amphiboles synthesized in this study

Duration (h)	119	144	95	99	95	305	94	73	330	288
T (°C)/P (GPa)	950/1.0	950/1.1	950/1.2	900/0.8	900/1.0	900/1.1	900/1.2	900/1.4	800/0.9	800/1.0
No. of analyses (1σ)	51	18	45	21	36	10	22	16	13	3
SiO_2	40.72 (51)	40.50 (57)	40.54 (85)	41.88 (89)	41.64 (55)	40.81 (34)	41.02 (61)	41.43 (84)	41.83 (83)	42.05 (28)
Al_2O_3	14.62 (53)	14.57 (45)	14.77 (77)	14.32 (58)	14.24 (64)	14.23 (25)	15.12 (62)	15.16 (62)	12.98 (52)	14.02 (52)
FeO	15.21 (55)	15.71 (34)	14.65 (48)	16.11 (55)	16.47 (43)	15.46 (36)	16.22 (43)	15.80 (71)	16.72 (60)	16.30 (25)
MgO	11.18 (33)	10.85 (30)	11.06 (29)	10.13 (53)	10.36 (26)	10.94 (25)	10.14 (19)	10.34 (33)	9.65 (35)	9.75 (06)
MnO	0.18 (04)	0.15 (05)	0.15 (05)	0.24 (03)	0.24 (02)	0.10 (02)	0.18 (06)	0.12 (04)	0.26 (06)	0.27 (03)
TiO_2	3.35 (21)	2.75 (23)	2.68 (26)	2.56 (12)	2.62 (14)	2.17 (08)	2.42 (22)	2.17 (20)	2.04 (18)	1.91 (21)
CaO	10.14 (43)	10.04 (53)	10.05 (61)	10.83 (49)	10.74 (51)	10.60 (16)	10.19 (37)	9.99 (28)	11.22 (45)	10.88 (07)
Na_2O	3.10 (25)	2.81 (17)	2.89 (23)	2.41 (15)	2.38 (16)	2.66 (12)	2.73 (10)	2.92 (11)	2.32 (15)	2.40 (08)
K_2O	0.11 (06)	0.13 (02)	0.14 (02)	0.13 (01)	0.13 (01)	0.15 (01)	0.14 (01)	0.15 (02)	0.14 (02)	0.10 (02)
Total	98.60 (77)	97.51 (85)	96.93 (83)	98.61 (68)	98.82 (53)	97.13 (98)	98.14 (95)	98.09 (89)	97.16 (114)	97.67 (22)
Formula proportions of cations based on 23 O atoms										
Si	5.99 (06)	6.03 (08)	6.04 (10)	6.16 (11)	6.09 (02)	6.12 (08)	6.07 (07)	6.11 (09)	6.28 (09)	6.25 (05)
Al	2.53 (09)	2.56 (08)	2.60 (14)	2.48 (10)	2.51 (04)	2.47 (11)	2.64 (10)	2.64 (09)	2.30 (08)	2.46 (09)
Fe^{2+}	1.69 (90)	1.77 (04)	1.65 (06)	1.79 (07)	1.74 (04)	1.83 (05)	1.81 (05)	1.76 (09)	1.89 (08)	1.83 (03)
Fe^{3+}	0.18 (00)	0.19 (00)	0.18 (00)	0.19 (00)	0.19 (00)	0.20 (00)	0.20 (00)	0.19 (00)	0.20 (00)	0.20 (00)
Mg	2.45 (09)	2.41 (06)	2.46 (06)	2.22 (12)	2.44 (06)	2.27 (05)	2.23 (04)	2.27 (07)	2.16 (07)	2.16 (01)
Mn	0.02 (00)	0.02 (01)	0.02 (01)	0.03 (00)	0.01 (00)	0.03 (00)	0.02 (01)	0.02 (01)	0.03 (01)	0.03 (00)
Ti	0.37 (02)	0.31 (03)	0.30 (03)	0.28 (01)	0.24 (01)	0.29 (02)	0.27 (03)	0.24 (03)	0.23 (02)	0.21 (02)
Ca	1.60 (06)	1.60 (08)	1.61 (07)	1.71 (08)	1.70 (03)	1.69 (08)	1.61 (06)	1.58 (05)	1.80 (08)	1.73 (01)
Na	0.88 (07)	0.81 (04)	0.84 (07)	0.69 (04)	0.77 (03)	0.68 (04)	0.78 (03)	0.84 (03)	0.68 (04)	0.69 (02)
K	0.02 (01)	0.03 (00)	0.03 (00)	0.02 (01)	0.03 (00)	0.02 (01)	0.03 (01)	0.03 (00)	0.03 (00)	0.02 (00)
Sum	15.74 (05)	15.71 (04)	15.70 (06)	15.58 (09)	15.72 (03)	15.61 (05)	15.66 (04)	15.67(06)	15.60 (09)	15.57 (04)

TABLE 2—*Continued*

Duration (h)	240	765	1172	959	398	1118	720	1220	168	549
T (°C)/P (GPa)	700/1.4	700/1.4	700/1.4	700/1.4	700/1.6	700/1.6	700/1.6	700/1.6	700/1.8	700/1.8
No. of analyses (1σ)	6	14	56	50	24	45	16	45	25	60
SiO_2	43.04 (24)	43.55 (46)	44.66 (78)	43.90 (56)	44.56 (82)	43.79 (83)	43.31 (94)	44.25 (72)	45.84 (86)	45.32 (72)
Al_2O_3	13.47 (28)	13.39 (91)	12.79 (58)	13.52 (63)	13.18 (60)	15.01 (109)	13.73 (76)	13.33 (64)	12.64 (56)	13.49 (47)
FeO	14.95 (76)	16.20 (57)	15.53 (53)	15.52 (40)	15.77 (60)	15.46 (45)	15.44 (63)	15.97 (49)	14.92 (86)	15.35 (46)
MgO	9.47 (23)	9.51 (24)	9.77 (34)	9.49 (33)	9.69 (42)	9.31 (42)	9.40 (49)	9.66 (31)	10.10 (90)	9.90 (21)
MnO	0.29 (05)	0.26 (02)	0.24 (04)	0.23 (04)	0.24 (05)	0.24 (02)	0.20 (03)	0.27 (03)	0.23 (04)	0.18 (06)
TiO_2	1.03 (19)	1.37 (49)	1.17 (35)	1.21 (29)	1.22 (58)	1.33 (36)	1.04 (25)	1.10 (34)	1.09 (37)	1.04 (28)
CaO	9.87 (32)	10.79 (54)	10.12 (38)	11.15 (31)	9.94 (78)	9.82 (44)	10.68 (67)	10.22 (34)	9.01 (35)	9.07 (28)
Na_2O	2.94 (17)	2.42 (49)	2.86 (21)	2.29 (18)	2.87 (42)	2.96 (46)	2.97 (76)	3.23 (18)	3.03 (26)	3.36 (24)
K_2O	0.20 (03)	0.17 (02)	0.18 (01)	0.16 (01)	0.16 (07)	0.23 (03)	0.16 (01)	0.20 (02)	0.18 (09)	0.21 (03)
Total	95.25 (71)	97.65 (78)	97.33 (82)	97.48 (72)	97.64 (92)	98.15 (67)	96.94 (96)	98.22 (62)	97.04 (146)	97.93 (89)
Formula proportions of cations based on 23 O atoms										
Si	6.49 (03)	6.44 (12)	6.59 (10)	6.48 (07)	6.56 (08)	6.40 (14)	6.44 (10)	6.50 (09)	6.73 (08)	6.62 (06)
Al	2.40 (06)	2.34 (25)	2.23 (09)	2.35 (11)	2.29 (10)	2.59 (23)	2.41 (12)	2.31 (12)	2.19 (07)	2.32 (08)
Fe^{2+}	1.70 (09)	1.81 (08)	1.73 (07)	1.73 (06)	1.75 (08)	1.71 (05)	1.73 (08)	1.77 (06)	1.65 (12)	1.69 (06)
Fe^{3+}	0.18 (00)	0.20 (00)	0.19 (00)	0.19 (00)	0.19 (00)	0.18 (00)	0.19 (00)	0.19 (00)	0.18 (00)	0.18 (00)
Mg	2.13 (05)	2.10 (09)	2.15 (07)	2.09 (08)	2.13 (09)	2.03 (13)	2.08 (07)	2.12 (07)	2.21 (18)	2.15 (05)
Mn	0.04 (01)	0.03 (00)	0.03 (01)	0.03 (01)	0.03 (01)	0.03 (00)	0.03 (00)	0.03 (00)	0.03 (01)	0.02 (01)
Ti	0.12 (02)	0.15 (03)	0.13 (04)	0.13 (06)	0.14 (06)	0.15 (04)	0.12 (03)	0.12 (04)	0.12 (04)	0.11 (03)
Ca	1.60 (05)	1.71 (07)	1.60 (07)	1.76 (06)	1.57 (13)	1.54 (08)	1.70 (12)	1.61 (05)	1.42 (06)	1.42 (04)
Na	0.86 (05)	0.69 (06)	0.82 (06)	0.66 (05)	0.82 (12)	0.84 (14)	0.86 (22)	0.92 (05)	0.86 (07)	0.95 (07)
K	0.04 (01)	0.03 (01)	0.03 (00)	0.03 (00)	0.03 (01)	0.04 (01)	0.03 (00)	0.04 (00)	0.03 (02)	0.04 (01)
Sum	15.55 (04)	15.50 (05)	15.50 (09)	15.46 (06)	15.49 (06)	15.51 (10)	15.59 (12)	15.61 (07)	15.42 (10)	15.51 (07)

Apparatus

Experiments were conducted in a piston-cylinder apparatus using a 2.54 cm diameter furnace assembly for experiments at $P \leq 2.0$ GPa, and a 1.91 cm diameter assembly for those at $P > 2.0$ GPa. A NaCl-pyrex glass-graphite furnace assembly was employed for experiments at $T > 850$ °C, and a NaCl-graphite assembly was used for those at $T < 800$ °C. The furnace assembly design ensures isotropic pressure distribution and a smooth thermal gradient. To minimize friction between the assembly and pressure vessel, lead foil was wrapped around the furnace/sample cell, and the cylinder walls were lubri-cated with dry MoS_2. Pressure corrections resulting from the strength of the assembly and friction between the assembly and cylinder are negligible. Pressures were calibrated against the phase transitions albite = jade-ite+quartz (Liu and Bohlen 1995) and quartz = coesite (Bohlen and Boettcher 1982). Temperatures were measured with $Pt-Pt_{90}Rh_{10}$ thermocouples isolated from the capsule by a platinum shield. No pressure correction was applied to the emf of the thermocouples. The precision of P and T measurement is ±10 MPa, and ±2 °C, and accuracy is estimated to be ±50 MPa, and ±10 °C, respectively. For all experiments, temperatures were main-

TABLE 2—*Continued*

241 800/1.2 34	262 800/1.4 45	284 800/1.6 14	217 800/1.8 20	138 800/2.0 18	336 750/1.0 11	669 700/0.8 22	573 700/1.0 32	500 700/1.2 29	500 700/1.2 5	264 700/1.2 14
42.23 (90)	41.75 (82)	42.32 (69)	42.63 (51)	43.27 (38)	45.02 (111)	43.96 (51)	43.47 (72)	43.62 (86)	44.05 (63)	42.67 (62)
14.68 (82)	15.79 (65)	15.17 (72)	15.01 (79)	14.43 (72)	11.82 (105)	11.93 (73)	12.84 (97)	13.70 (87)	12.50 (82)	13.27 (22)
16.07 (64)	15.72 (68)	15.26 (56)	15.45 (68)	15.99 (61)	16.34 (54)	16.78 (33)	16.50 (52)	16.22 (71)	16.99 (95)	15.28 (56)
9.15 (34)	8.66 (27)	9.43 (55)	9.41 (48)	9.43 (41)	9.82 (33)	9.67 (31)	9.51 (30)	9.27 (29)	9.50 (12)	9.17 (35)
0.25 (05)	0.23 (04)	0.25 (06)	0.22 (03)	0.23 (06)	0.25 (06)	0.20 (07)	0.15 (04)	0.16 (04)	0.21 (08)	0.27 (04)
1.73 (31)	1.73 (40)	1.52 (24)	1.30 (37)	1.23 (16)	1.35 (30)	1.19 (27)	1.26 (41)	1.24 (27)	1.40 (23)	1.25 (46)
10.57 (39)	10.19 (41)	10.07 (29)	9.44 (26)	8.64 (62)	11.29 (26)	11.52 (32)	11.68 (28)	11.19 (27)	11.28 (51)	11.04 (42)
2.04 (12)	2.46 (13)	2.64 (22)	2.99 (47)	2.78 (19)	1.89 (24)	1.71 (09)	1.89 (28)	2.16 (25)	1.81 (06)	2.33 (39)
0.14 (02)	0.15 (03)	0.16 (02)	0.16 (04)	0.16 (02)	0.15 (08)	0.14 (02)	0.14 (01)	0.15 (03)	0.11 (03)	0.14 (04)
96.86 (84)	96.68 (69)	96.81 (117)	96.62 (77)	96.15 (79)	97.93 (71)	97.11 (68)	97.44 (74)	97.71 (93)	97.84 (117)	95.42 (81)
Formula proportions of cations on 23 O atoms										
6.29 (10)	6.22 (10)	6.29 (06)	6.34 (08)	6.45 (05)	6.63 (13)	6.56 (07)	6.46 (10)	6.44 (06)	6.52 (09)	6.45 (04)
2.58 (15)	2.78 (12)	2.66 (11)	2.63 (14)	2.54 (12)	2.05 (91)	2.10 (12)	2.25 (18)	2.39 (04)	2.18 (15)	2.37 (12)
1.81 (08)	1.77 (09)	1.71 (07)	1.74 (01)	1.80 (07)	1.82 (06)	1.89 (04)	1.85 (07)	1.81 (06)	1.90 (09)	1.74 (12)
0.20 (00)	0.19 (00)	0.18 (00)	0.19 (00)	0.19 (00)	0.20 (00)	0.20 (00)	0.20 (00)	0.20 (00)	0.20 (00)	0.19 (00)
2.03 (08)	1.92 (06)	2.09 (10)	2.09 (11)	2.10 (10)	2.16 (07)	2.15 (07)	2.11 (06)	2.04 (08)	2.10 (07)	2.07 (05)
0.03 (01)	0.03 (01)	0.03 (01)	0.03 (00)	0.03 (01)	0.03 (01)	0.03 (01)	0.02 (01)	0.02 (01)	0.03 (00)	0.04 (01)
0.19 (03)	0.19 (04)	0.17 (03)	0.15 (04)	0.14 (03)	0.15 (03)	0.13 (03)	0.14 (04)	0.14 (05)	0.16 (03)	0.14 (03)
1.69 (07)	1.63 (07)	1.60 (05)	1.50 (04)	1.38 (10)	1.78 (03)	1.84 (05)	1.86 (04)	1.77 (07)	1.79 (05)	1.79 (08)
0.59 (04)	0.71 (04)	0.76 (06)	0.86 (14)	0.80 (06)	0.54 (07)	0.50 (03)	0.55 (09)	0.62 (12)	0.52 (07)	0.68 (02)
0.03 (00)	0.03 (01)	0.03 (01)	0.03 (01)	0.03 (01)	0.03 (02)	0.03 (00)	0.03 (00)	0.03 (01)	0.02 (01)	0.03 (01)
15.44 (06)	15.47 (06)	15.52 (05)	15.55 (06)	15.46 (06)	15.38 (09)	15.42 (03)	15.46 (06)	15.45 (10)	15.41 (07)	15.49 (05)

TABLE 2—*Continued*

720 700/1.8 46	1101 700/1.8 45	741 700/2.0 15	552 650/2.2 6	1392 650/2.2 18	1630 650/2.2 3	840 650/2.2 3	1392 650/2.2 6
45.20 (68)	44.99 (52)	45.05 (83)	48.18 (85)	48.25 (52)	48.56 (50)	48.11 (146)	49.10 (80)
12.41 (61)	12.84 (58)	13.98 (65)	11.71 (101)	11.29 (84)	11.68 (74)	11.76 (133)	11.45 (59)
15.59 (55)	15.33 (52)	15.74 (133)	16.49 (57)	15.28 (102)	15.52 (123)	14.01 (188)	14.31 (198)
9.73 (37)	9.97 (25)	9.81 (73)	10.83 (60)	10.86 (41)	10.89 (32)	10.21 (86)	10.32 (93)
0.24 (05)	0.21 (05)	0.17 (06)	0.24 (01)	0.23 (03)	0.24 (05)	0.18 (03)	0.21 (04)
0.98 (28)	1.04 (30)	0.91 (18)	0.80 (57)	0.60 (23)	0.57 (05)	0.72 (47)	0.59 (15)
8.97 (35)	8.99 (35)	8.79 (28)	6.80 (68)	6.45 (82)	6.32 (131)	8.03 (135)	7.67 (174)
3.44 (27)	3.56 (24)	3.87 (53)	3.15 (21)	3.37 (25)	3.43 (30)	3.44 (80)	3.74 (23)
0.23 (02)	0.24 (03)	0.18 (02)	0.29 (04)	0.27 (04)	0.22 (05)	0.26 (08)	0.21 (06)
96.84 (82)	97.18 (90)	98.50 (101)	98.47 (136)	96.60 (84)	97.43 (25)	96.71 (47)	97.62 (73)
Formula proportions of cations based on 23 O atoms							
6.70 (09)	6.63 (06)	6.56 (08)	6.94 (11)	7.05 (07)	7.03 (07)	7.01 (16)	7.08 (08)
2.17 (13)	2.23 (09)	2.40 (10)	1.99 (15)	1.94 (14)	1.99 (13)	2.02 (23)	1.95 (08)
1.74 (09)	1.71 (06)	1.73 (17)	1.79 (08)	1.68 (13)	1.70 (16)	1.54 (25)	1.56 (28)
0.19 (00)	0.18 (00)	0.19 (00)	0.19 (00)	0.18 (00)	0.18 (00)	0.17 (00)	0.17 (00)
2.15 (12)	2.19 (06)	2.13 (15)	2.33 (12)	2.36 (09)	2.35 (06)	2.22 (20)	2.22 (22)
0.03 (01)	0.03 (01)	0.02 (01)	0.03 (06)	0.03 (00)	0.03 (01)	0.02 (00)	0.03 (01)
0.11 (03)	0.12 (03)	0.10 (02)	0.09 (00)	0.07 (03)	0.06 (01)	0.08 (05)	0.06 (02)
1.42 (09)	1.42 (05)	1.37 (06)	1.05 (11)	1.01 (13)	0.98 (20)	1.25 (20)	1.19 (35)
0.99 (11)	1.02 (07)	1.09 (14)	0.88 (06)	0.95 (13)	0.96 (09)	0.97 (22)	1.05 (09)
0.04 (00)	0.05 (01)	0.03 (00)	0.05 (01)	0.05 (01)	0.04 (01)	0.05 (01)	0.04 (01)
15.53 (11)	15.57 (06)	15.62 (11)	15.35 (06)	15.33 (04)	15.32 (02)	15.33 (10)	15.34 (07)

tained within ±2 °C. Pressures fluctuated as reaction proceeded; whenever detected, *P* was adjusted to the original value. The maximum variation of pressures in these experiments was 40 MPa.

Oxidation state

Oxygen fugacity was buffered using the standard double-capsule technique (Eugster 1957), with either 3.0 mm outside diameter (o.d.) $Ag_{70}Pd_{30}$ or 1.6 mm o.d. $Ag_{80}Pd_{20}$ as the inner capsule, 5.0 mm Au as the outer capsule, and fayalite-magnetite-quartz (FMQ) plus a small amount of H_2O (4 wt%) as the buffer assemblage. By controlling the oxidation state, we attempted to simulate the environment of the upper part of subducting, relatively unaltered oceanic crust; appropriate conditions are thought by many investigators to approximate that defined by FMQ (Wood and Virgo 1989; Wood et al. 1990). Fayalite was synthesized by reacting equimolar Fe and natural, HNO_3-leached Brazilian quartz. Optical, X-ray diffraction, and EMPA indicate that the fayalite is homogeneous and stoichiometric. Fayalite, natural Brazilian quartz, and reagent grade Fe_3O_4 were mixed in the molar ratio 1:1:1.5. At the conclusion of every experiment, the buffer assemblage was checked microscopically to ensure the presence of
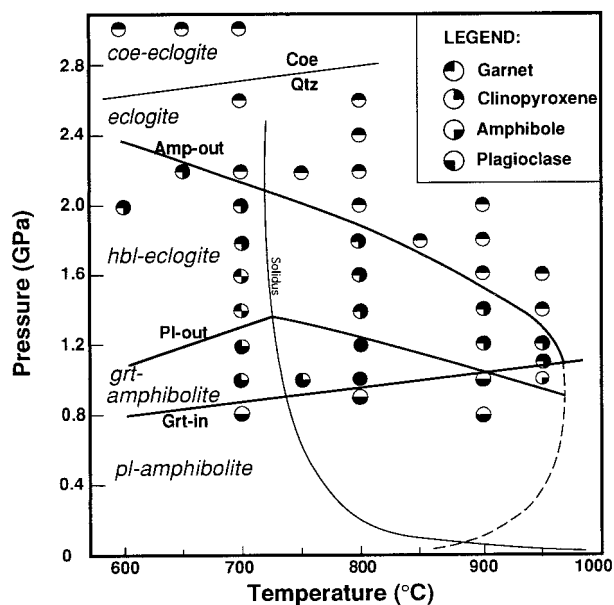
FIGURE 1. Petrogenetic grid for the amphibolite to eclogite transformation in the MORB basalt-H₂O system, after Liu et al. (1996). Abbreviations: amp = amphibole; coe = coesite; grt = garnet; hbl = hornblende; pl = plagioclase; qtz = quartz.

all buffer phases, including water (buffer assemblages were damp).

At pressures greater than the equilibrium fayalite+quartz = ferrosilite (Bohlen et al. 1980; Bohlen 1984), ferrosilite replaced fayalite; at pressures greater than the quartz = coesite transition (Bohlen and Boettcher 1982), coesite replaced quartz in the buffer assemblage. The phase transitions affect the f_{O_2} only slightly: the fugacity of O_2 for ferrosilite-magnetite-quartz is 0.1 to 0.2 log units greater than that defined by FMQ, and the fugacity of O_2 for ferrosilite-magnetite-coesite is 0.1 to 0.2 log unit less than that defined by the assemblage ferrosilite-magnetite-quartz.

Fluid

Estimated contents of H₂O are 1–2 wt% in hydrated basalt and amphibolite (Thompson 1992), 3 wt% in greenschist, and up to 6–7 wt% in lawsonite-bearing blueschist (Peacock 1990, 1992). Petrologic studies suggest that some hydrous minerals including clinozoisite, phengite, and amphibole are primary metamorphic phases at high pressures, and that H₂O or saline aqueous solution is the most important fluid constituent in eclogite-facies metamorphism (Ernst 1972b; Holland 1979; Sorensen and Grossman 1993; Selverstone et al. 1993). A total of 4 wt% of H₂O was used in most experiments to simulate closely conditions during subduction under subsolidus and near-solidus conditions. We loaded 0.80 to 1.20 ml H₂O together with 20–30 mg of starting mixture into silver-palladium capsules. Welded capsules, together with the buffer, were put into 5.0 mm o.d. gold capsules that

were then welded shut. Weight loss of water, determined after drying the synthesized products, confirmed that all experiments were H₂O saturated.

Experimental duration

Due to slow reaction rates in the basalt-H₂O system under the *P-T* conditions investigated, experiments were conducted on average 4, 7, 30, and 50 d at 900, 800, 700, and 650 °C (see Table 2), in contrast to most previous studies reported in the literature, which lasted several hours to 1–2 d. We conducted experiments at the same *P-T* conditions over different lengths of time to monitor the change in modal proportion and compositions of minerals in the synthesized products. Long experiments were found to be necessary to obtain consistent phase relations, especially at subsolidus temperatures. Such durations also ensured that all minerals were sufficiently coarse-grained that they could be identified optically and analyzed by the electron microprobe. Compositional homogeneity was evaluated using BSE imagery, X-ray maps, and line-profile analyses.

Analytical methods

All phases were positively identified by optical microscopy and a JEOL 8900 electron-microprobe analyzer. Samples were mounted in epoxy, and were polished for 4 h using 6 to 0.3 μm diamond paste. The microprobe was operated at 15 kV, with a focused beam 1–2 μm in diameter, operating at a current of 12 or 15 nA. Neither compositional zoning of phases nor Fe loss to the AgPd container walls was detected.

Phase equilibrium results

Amphibolite transforms to eclogite with increasing aqueous fluid pressure through three continuous equilibria: crystallization of garnet, breakdown of plagioclase, and decomposition of Ca-amphibole (Liu et al. 1996; Liu 1997). These reaction boundaries divide *P-T* space into four regions corresponding to the amphibolite, garnet-amphibolite, hornblende-eclogite, and eclogite facies, as illustrated in Figure 1. Condensed mineral assemblages (plus a Ti-phase) characterizing the four *P-T* regions with increasing *P* are (1) at *T* ≤ 700 °C, plagioclase+amphibole+quartz, garnet+ plagioclase+amphibole+quartz, garnet+amphibole ±clinopyroxene+quartz, and garnet+clinopyroxene+quartz or coesite; and, (2) at *T* ≥ 750 °C, plagioclase+amphibole± clinopyroxene+melt, garnet+plagioclase+amphibole± clinopyroxene+melt, garnet+amphibole+clinopyroxene +melt, and garnet+clinopyroxene+melt. The H₂O-saturated solidus of the system is located between 700–750 °C at 1.0–2.2 GPa.

Accessory titanite, ilmenite, and rutile are Ti-rich phases coexisting with the silicates and/or melt. Synthesis fields for these Ti-phases are delineated in Figure 2: rutile is stable at high pressures (*P* > 1.6 GPa at *T* ≥ 800 °C, *P* > 1.4 GPa at 700 °C), ilmenite is stable at low pressures and high temperatures (*P* < 1.6 GPa at *T* ≥ 800 °C), and titanite is stable at relatively low pressures and
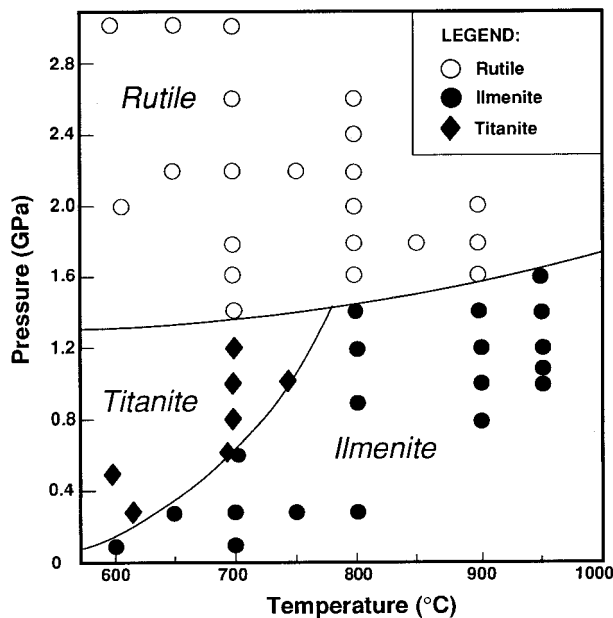
FIGURE 2. Synthesis fields and presumed stability relations of Ti-phases for the MORB basalt-H_2O system, after Liu et al. (1996).

low temperatures ($P < 1.4$ GPa at 700 °C). Inasmuch as these phases have different compositions, the field boundaries shown must be multivariant zones of finite but unmeasured *P-T* width; these zones should be sensitive to bulk-rock compositional variations, especially the activities of Mg, Fe, Ca, Si, H, O, and C. The *P-T* region depicted for titanite growth in Figure 2 appears to be unrealistically broad, based on petrologic experience. However, the fields illustrated are topologically consistent with natural occurrence of Ti-phases: rutile, ilmenite, and titanite are common in eclogite+hornblende-eclogite, granulite+high-rank amphibolite, and greenschist+low-rank amphibolite facies, respectively.

Compositions of synthesized amphiboles produced in this study are listed in Table 2. Compositions of coexisting synthetic phases are presented in appendices as follows: Appendix 1, garnet; Appendix 2, plagioclase; Appendix 3, clinopyroxene; and Appendix 4, melt.

GARNET-IN PHASE BOUNDARY

The crystallization of garnet is a pressure-sensitive reaction. At subsolidus temperatures, garnet may be produced by consumption of anorthite and pargasite components of Ca-amphibole, producing albite-rich plagioclase and tremolite-rich amphibole along with garnet (Mäder and Berman 1992):

anorthite+pargasite = garnet+tremolite+albite.
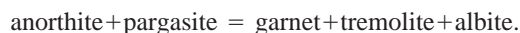
At supersolidus temperatures, garnet is produced by consumption of amphibole and plagioclase through the reaction (Wolf and Wyllie 1993):

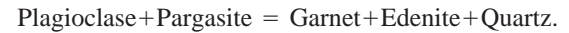plagioclase+amphibole = garnet±clinopyroxene+melt.
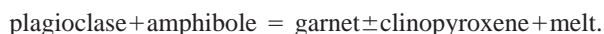
At low pressures ($P \leq 1.0$ GPa) and high temperatures ($T \geq 800$ °C), incongruent melting of plagioclase and Ca-amphibole produces clinopyroxene and melt by a temperature-sensitive reaction (Spear 1981; Wolf and Wyllie 1993):

plagioclase+Ca-amphibole = clinopyroxene+melt.

PLAGIOCLASE-OUT PHASE BOUNDARY

At subsolidus temperatures and increasing pressures, plagioclase is consumed by reaction with Ca-amphibole:

Plagioclase+Pargasite = Garnet+Edenite+Quartz.

Clinopyroxene was not produced at 700 °C, 1.4 GPa, for example, where plagioclase breaks down. Instead, a garnet+Ca-amphibole+rutile+quartz assemblage replaces a garnet+plagioclase+Ca-amphibole+titanite (+quartz) assemblage. This reaction is different from the plagioclase-out reaction in the anhydrous system (Green and Ringwood 1967), where plagioclase breaks down to yield jadeitic pyroxene and quartz. The plagioclase-out boundary in the hydrous MORB system therefore does not represent the boundary for eclogite facies.

At supersolidus temperatures, formation of clinopyroxene by the incongruent melting of plagioclase and Ca-amphibole results in the decomposition of plagioclase:

plagioclase+Ca-amphibole+H_2O = clinopyroxene+melt.

Plagioclase disappears between 1.0 and 1.1 GPa at 900 °C, between 1.2 and 1.4 GPa at 800 °C, and between 1.2 and 1.4 GPa at 700 °C. The *P-T* slope of the plagioclase-out curve above the solidus is negative (Fig. 1), indicating the consumption of aqueous fluid during the production of hydrous melt; this curve is consistent with the results of Hill and Boettcher (1970) and Wolf and Wyllie (1993).

CA-AMPHIBOLE EQUILIBRIA

Ca-amphibole transforms to anhydrous solids+H_2O over a relatively narrow *P-T* range in a continuous but abrupt fashion at subsolidus temperatures, whereas it diminishes slowly over a broad range of conditions at supersolidus temperatures. At 700 °C, for example, Ca-amphibole starts to break down at 1.6–1.8 GPa to yield jadeitic pyroxene+garnet, and has decomposed completely at 2.2 GPa. In contrast, Ca-amphibole dehydrates gradually over a broad range of conditions at supersolidus temperatures. At 800 °C, for example, it begins to devolatilize at 0.8 GPa, and has decomposed completely at 2.0 GPa. An important amount of H_2O is released at subsolidus temperatures in a rather narrow pressure range; this devolatilization may have a significant effect on initiating partial melting of the upper mantle, and on catalyzing the amphibolite → eclogite transition. As shown in Figure 1, the assemblage garnet+clinopyroxene+Ca-amphibole+quartz breaks down to garnet+clinopyroxene+quartz+H_2O at subsolidus temperatures, and garnet+clinopyroxene+Ca-amphibole+melt transforms to garnet+clinopyroxene+melt+H_2O at supersolidus temperatures. Ca-amphibole decomposes between

1.2 and 1.4 GPa at 950 °C, between 1.4 and 1.6 GPa at 900 °C, between 1.8 and 2.0 GPa at 800 °C, between 2.0 and 2.2 GPa at 700 °C, between 2.2 and 3.0 GPa at 650 °C, and <3.0 GPa at 600 °C.

Of critical importance is the fact that high-pressure experiments have defined a negative P-T slope of -2.8 MPa/°C for the amphibole-out reaction. This negative P-T slope reflects the fact that the higher entropy assemblage garnet+clinopyroxene+minor aqueous fluid possesses a smaller aggregate volume than the equivalent amount of Ca-amphibole. We performed two-stage experiments at 800 °C to reverse the amphibole-out reaction. The amphibole-bearing assemblage of garnet+clinopyroxene+Ca-amphibole+melt was synthesized at 1.8 GPa, then P was raised isothermally to 2.0 GPa and held for 5 d. The Ca-amphibole decomposed completely, yielding garnet+clinopyroxene+melt. However, it proved much more difficult to reverse the reaction and to produce Ca-amphibole from the high-pressure side (the amphibole-in reaction). Ca-amphibole failed to crystallize at 1.8 GPa in experiments lasting 4 to 8 d from an amphibole-free crystalline assemblage synthesized at 2.0 GPa. This may reflect the difficulty of nucleation of amphibole from the crystalline materials. At a lower pressure of 1.6 GPa, Ca-amphibole did grow from an amphibole-free assemblage synthesized at 2.0 GPa. This bracket, although wide, is consistent with the lengthy synthesis experimental results.

Ca-AMPHIBOLE COMPOSITIONS

Amphibole crystals synthesized at 650–950 °C are euhedral, prismatic, coarse-grained (5–7 × 10–15 μm), and pleochroic from pale green to greenish brown. Petrographic and electron-microprobe studies have documented its chemical homogeniety.

Recalculation of amphibole structural formulas

The structural formulas of synthetic amphiboles were calculated on an anhydrous basis assuming 23 O atoms per half unit cell, with the general form $A_{0-1}B_2C_5T_8O_{22}(OH)_2$, where A = a single 10–12 fold-coordinated A site, B = 2 six to eightfold-coordinated M4 sites, C = 5 M1, M3, and M2 octahedral sites, and T = 8 tetrahedral sites (Leake 1978; Leake et al. 1997). This expression represents one formula unit.

The IMA classification utilizes values of both Mg/(Mg+Fe^{2+}) and Fe^{3+}/(Fe^{3+}+Al) as discrimination parameters. Because the electron microprobe cannot distinguish between Fe^{2+} and Fe^{3+}, it is necessary to estimate the amounts of these cations in order to characterize the amphibole solid solutions (see below for our solution to this problem). We followed the IMA scheme for site assignment of cations: (1) tetrahedral (T) sites: sum T to 8.00 using Si, then Al, then Ti; (2) octahedral (M1+M2+M3) sites: sum C to 5.00 using excess Al, Fe^{3+}, Ti, Mg, Fe^{2+}, and Mn; (3) M4 sites: sum B to 2.00 using excess Fe^{2+}, Mn, Mg, then Ca, then Na; and (4), A site: excess Na from (3), then all K.
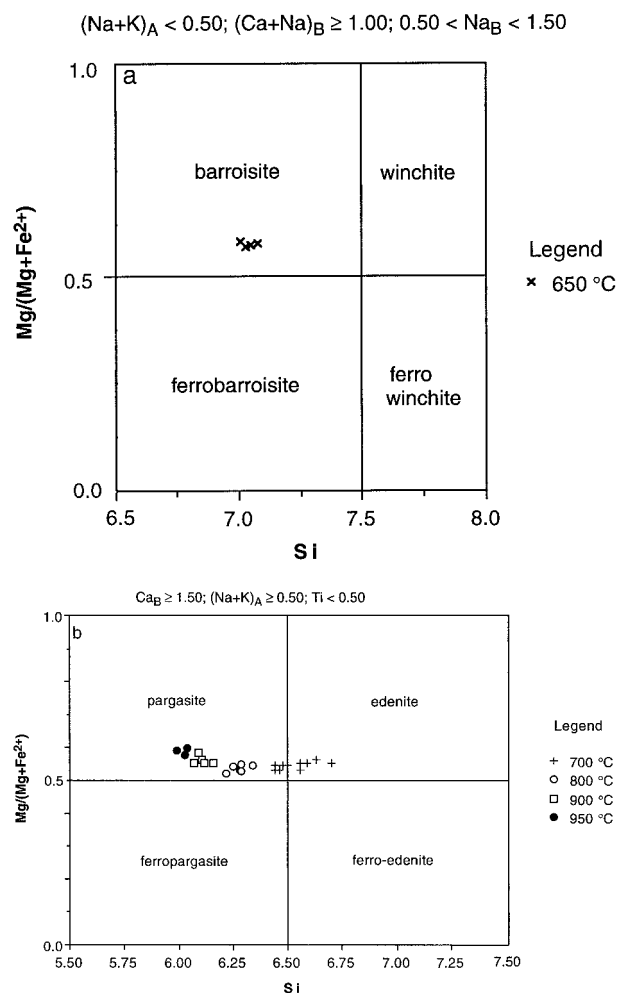

FIGURE 3. Compositional variation of synthetic Ca-amphiboles at 0.8–2.2 GPa as a function of temperature: (a) 650 °C; (b) 700–950 °C. Data are from Liu (1997). Cation proportions are shown for one formula unit. Amphibole classification is that of Leake et al. (1997).

Assuming all Fe is Fe^{2+}, we calculated the structural formula of the synthesized Ca-amphiboles using the above cation assignment scheme. An analysis was rejected if one of the following criteria could not be met: tetrahedral site occupancy = 8.00 ± 0.02; octahedral site occupancy ≥ 4.98; excess octahedral cations+Ca occupancy ≤ 2.02; or A site occupancy ≤ 1.02. For the surviving data, we calculated amphibole structural formulas by adjusting their contents of Fe^{2+} and Fe^{3+}. Several such recalculation schemes for amphiboles are in common usage: (1) assume no Fe^{3+}, all Fe considered as Fe^{2+}; (2) total cations (excluding Ca, Na, and K) = 13 ; and (3), total cations (excluding Na and K) = 15. These recalculation schemes yield different values of Fe^{2+}/Fe^{3+} for the synthesized amphiboles. Of the three methods, (1) provides the minimum Fe^{3+} content (zero) and involves no adjustment of Fe^{2+}/Fe^{3+} for the EMPA; (2) has an implicit assumption that no Fe^{2+}, Mg, or Mn occurs in the M4
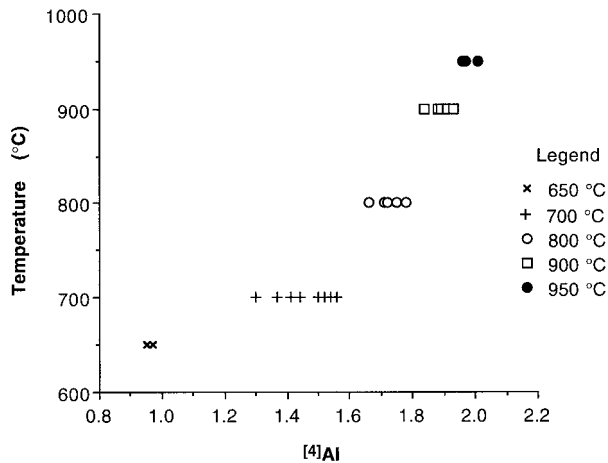
FIGURE 4. [4]Al contents of synthetic Ca-amphiboles as a function of temperature. Data are from Liu (1997). Cation proportions are shown for one formula unit.

FIGURE 5. Correlation of [4]Al and Ti contents of synthetic Ca-amphiboles. Data are from Liu (1997). Cation proportions are shown for one formula unit.

site, a good approximation for many Ca-amphiboles [although electron absorption spectra presented by Aldridge et al. (1982) demonstrate the presence of Fe^{2+} in the M4 sites of some Ca-amphiboles]; and (3) is appropriate for Fe-Mg amphiboles, where Ca and Na contents are low, and no Na occupies M4, and for Fe-Mg-Ca amphibole solid solutions (including many Ca-amphiboles). In addition to these approaches, Papike et al. (1974) proposed a fourth recalculation scheme that averages the Fe^{3+} obtained from (1) and (3) to derive an intermediate value.

We tested all these recalculation schemes. Schemes (1), (2), and the method of Papike et al. yielded consistent results for synthetic Ca-amphiboles, whereas scheme (3) gave high Fe^{3+} contents for barroisites. Spear (1981) measured the Fe^{3+} content of synthetic Ca-amphibole in one experiment at 707° C, 100 MPa, with f_{O_2} defined by the FMQ buffer in a basaltic system: the derived value of $Fe^{3+}/(Fe^{2+}+Fe^{3+})$ was 0.125. Popp et al. (1995) measured the Fe^{3+} content of a Ti-rich pargasite treated experimentally at 100 MPa employing the FMQ buffer: the $Fe^{3+}/(Fe^{2+}+Fe^{3+})$ value was 0.15 at 700 °C, and 0.20 at 900 °C. Accordingly, we adopted 0.125 as the Fe_2O_3/FeO_T ratio for recalculation of amphiboles in our experiments. Table 2 lists averages, standard deviations, and the number of analyses of amphibole (for simplicity, iron oxide is reported as FeO). The standard deviation, defined by $2\sigma = [(X_i - X)^2/n - 1]^{1/2}$, reflects the compositional variation of synthetic amphiboles.

The synthetic amphiboles change in composition from the sodic-calcic variety barroisite at 650 °C, 2.2 GPa, to Ca-amphibole at $T \geq 700$ °C (Fig. 3). The Si content of the Ca-amphibole decreases progressively with increasing temperature, from about 6.6 cations pfu in edenite at 700 °C to 6.3 in pargasite at 800 °C and above (at 900–950 °C, Si ~6.0–6.1). The Ti content of the amphibole increases with increasing temperature, from 0.07 cations
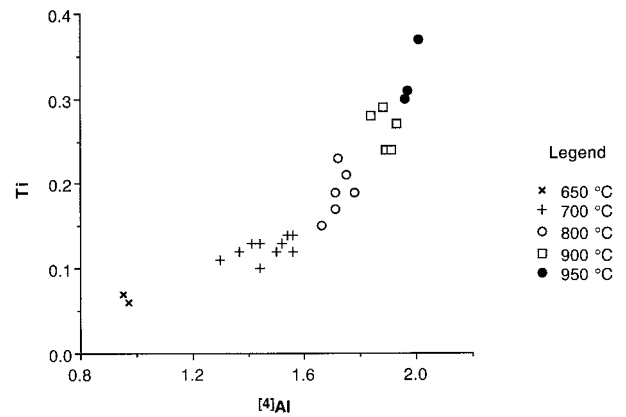
pfu at 650 °C, to 0.10–0.14 at 700 °C, 0.15–0.22 at 800 °C, 0.23–0.27 at 900 °C, and 0.30–0.35 at 950 °C.

Substitution mechanisms in the synthetic Ca-amphiboles

The compositional variations of amphiboles are described following Leake et al. (1997) and Thompson et al. (1982). Starting from the additive component tremolite, $Ca_2Mg_5Si_8O_{22}(OH)_2$, amphibole compositions can be described by four coupled-exchange vectors:

(1) the edenite substitution: $^{[A]}Na^{[4]}Al\,^{[A]}\square$-1$^{[4]}Si$-1
(2) the tschermakite substitution: $^{[6]}Al^{[4]}Al\,^{[6]}Mg-1^{[4]}Si$-1
(3) the Ti-tschermakite substitution: $^{[6]}Ti^{[4]}Al_2$ $^{[6]}Mg_{-1}^{[4]}Si_{-2}$
(4) the glaucophane substitution: $^{[M4]}Na^{[6]}Al$ $^{[M4]}Ca$-1$^{[6]}Mg$-1

and four single-ion-exchange vectors:

(5) $Fe^{2+}\,Mg_{-1}$
(6) $Mn\,Mg_{-1}$
(7) $Fe^{3+}\,Al_{-1}$
(8) $^{[A]}K\,^{[A]}Na$-1.

The isobaric [4]Al and Ti contents of synthetic Ca-amphiboles increase with increasing T (Figs. 4 and 5). At constant T, the saturation value of Ti in amphibole decreases very slightly with increasing P (Fig. 6). The [4]Al and Ti concentrations in synthetic amphibole are strongly correlated, as illustrated in a plot of [4]Al vs. Ti (Fig. 5). Because the computed [4]Al and [6]Al proportions of phases such as Ca-amphiboles are sensitive functions of both the normalization procedures and the EMPA for Si (a small percentage error in Si propagates as a large percentage error in the amphibole [4]Al/[6]Al), in practice we chose to consider total Al_2O_3 contents rather than either [4]Al or [6]Al. The Al_2O_3 and TiO_2 contents of amphibole are therefore potential thermometers.

Where Al substitutes for Si in the tetrahedral sites of amphibole through edenite, tschermakite, and Ti-tschermakite substitutions, the [4]Al content of amphibole should
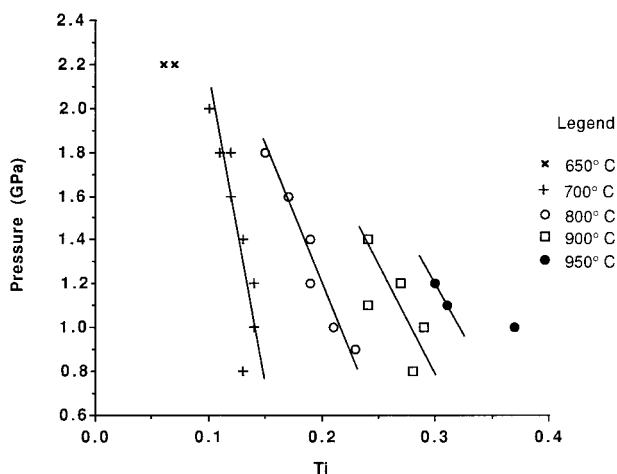
FIGURE 6. Ti contents of synthetic Ca-amphiboles as a function of temperature and pressure. Data are from Liu (1997). Cation proportions are shown for one formula unit.

FIGURE 7. Relationship of [6]Al+[M4]Na in synthetic Ca-amphiboles as a function of pressure. Data are from Liu (1997). Cation proportions are shown for one formula unit.

be equal to A site occupancy+[6]Al+Fe³⁺+2Ti. On a plot of [4]Al vs. A site occupancy+[6]Al+Fe³⁺+2Ti (not illustrated), our synthetic Ca-amphiboles fall on a straight line with a slope of unity that passes through the origin. The linear relationship demonstrates that the reaction mechanism in amphibole tetrahedral (and other) sites with increasing T involves edenite-, tschermakite-, and Ti-tschermakite-substitutions, a conclusion also reached by Spear (1981) on the basis of his experiments at $P < 0.5$ GPa, 500–920 °C.

The glaucophane substitution, on the other hand, is the major mechanism for the compositional variation of amphibole as P increases. The amounts of [M4]Na and [6]Al in the Ca-amphibole both increase with increasing P. In a plot of [6]Al+[M4]Na vs. P, all experimental data fall on a straight line, as shown by Figure 7. This substitution accounts for the generation of Na-Ca amphiboles at elevated pressures rather than Ca-amphiboles: barroisite at 650 °C vs. edenite solid solution at 700 °C. The glaucophane substitution is obviously disfavored by elevated temperatures, where pargasitic amphiboles are stable (Fig. 3b).

Comparison with other Ca-amphibole barometers and thermometers

In the subsolidus region where experiments produced coexisting quartz+plagioclase+Ca-amphibole (Fig. 1), our data may be compared with the geothermometer of Blundy and Holland (1990). Using their formulation, and the analyzed compositions of Ca-amphibole and plagioclase (Table 3; Liu 1997) synthesized in our experiments at 700 °C, we obtained the following nominal temperatures of crystallization (±38 °C): 699 °C at 0.8 GPa; 708 °C at 1.0 GPa; and 656 and 670 °C for two experiments at 1.2 GPa. Clearly, the Blundy and Holland (1990) expression faithfully reproduces our phase-equilibrium results within their stated temperature error limits. We judge that our analytical data are insufficiently accurate
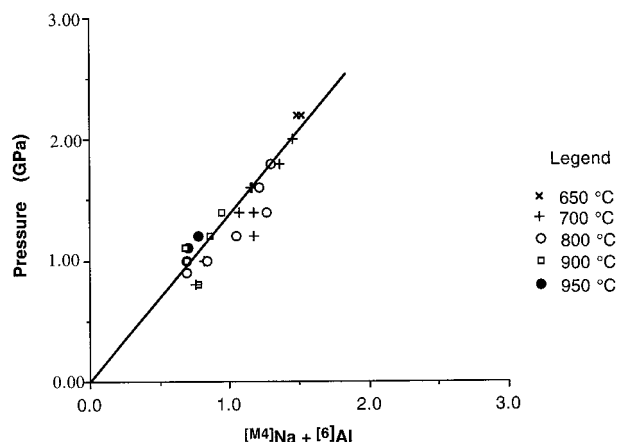
to justify employing the more sophisticated hornblende solid-solution model thermometer of Holland and Blundy (1994).

In similar fashion, but over a much broader P-T range, we evaluated the garnet-hornblende thermometer of Graham and Powell (1984). Utilizing their formulation, temperature disparities between experimentally controlled and calculated values were somewhat greater for seven coexisting synthesized mineral pairs, as follows: 950–909 °C at 1.2 GPa; 800–765 °C at 1.2 GPa; 800–875 °C at 1.4 GPa; 800–920 °C at 1.8 GPa; 800–898 °C at 2.0 GPa; 700–713 °C at 1.8 GPa; and 650–604 °C at 2.2 GPa. A portion of these differences may be attributable to imprecision in our microprobe analyses, and/or failure to achieve the equilibrium composition, especially for the garnet.

COMBINATION OF NEW DATA WITH PREVIOUS WORK

Comparable experimental investigations on natural rocks of basaltic bulk-rock chemistry that produced Ca-amphiboles have been carried out by numerous workers, employing similar, controlled f_{O_2} ranges (Ni-NiO; FMQ). In an attempt to maximize the use of equilibrium assemblages, only experiments of relatively long duration were selected. Phase equilibrium and Ca-amphibole analytical (Al+Ti) data are available for investigations of MORB-type bulk compositions as follows: Helz (1973, 1979); Liou et al. (1974); Spear (1981); Apted and Liou (1983); and Poli (1993). In all, 41 data sets were obtained from the literature, and corresponding values for Al and Ti are summarized in Table 3. Ca-amphiboles crystallized from natural andesitic/dacitic bulk compositions or from basalts subjected to extremely oxidizing or reducing laboratory conditions, or to P-T values well above solidus temperatures were not considered because compositional variations (including high proportions of melt) appear to influence the partitioning of Al_2O_3 in the coexisting Ca-amphibole.

TABLE 3. Al₂O₃ and TiO₂ contents of Ca-amphiboles synthesized from MORB

T in °C	P in GPa	wt% Al_2O_3	wt% TiO_2
Liou et al. (1974)			
457	0.2	3.0	0.1
480	0.2	3.4	0.2
507	0.2	4.0	0.1
550	0.2	4.1	0.2
597	0.2	4.3	0.3
Apted and Liou (1983)			
525	0.5	5.1	0.4
650	0.5	7.8	0.6
525	0.7	3.8	0.2
675	0.7	10.2	0.6
Spear (1981)			
599	0.1	6.6	0.8
651	0.1	7.3	0.7
707	0.1	7.7	1.1
750	0.1	7.8	1.4
802	0.1	9.0	1.8
850	0.1	9.7	2.2
551	0.3	5.2	0.4
610	0.3	5.7	0.5
655	0.3	7.2	0.8
699	0.3	8.3	1.0
763	0.3	8.3	1.4
710	0.5	9.3	1.1
Liu (1997)			
700	0.8	11.9	1.2
900	0.8	14.3	2.6
700	1.0	12.8	1.3
750	1.0	11.8	1.4
800	0.9	13.0	2.0
800	1.0	14.0	1.9
900	1.0	14.2	2.6
950	1.0	14.6	3.4
900	1.1	14.2	2.2
950	1.1	14.6	2.8
700	1.2	13.2	1.3
800	1.2	14.7	1.7
900	1.2	15.1	2.4
950	1.2	14.8	2.7
700	1.4	13.3	1.2
800	1.4	15.8	1.7
900	1.4	15.2	2.2
700	1.6	13.8	1.2
800	1.6	15.2	1.5
700	1.8	12.8	1.0
800	1.8	15.0	1.3
700	2.0	14.0	0.9
800	2.0	14.4	1.2
650	2.2	11.6	0.7
Poli (1993)			
640	1.0	10.7	
550	1.2	9.0	
650	1.2	13.0	
550	1.4	9.5	
640	1.4	11.5	
650	1.6	13.3	
650	1.7	12.8	
650	1.8	12.5	
650	2.0	12.7	
Helz (1979)			
1000	0.50	12.2	3.2
955	0.78	12.3	2.8
1050	0.80	14.1	5.2
Helz (1973)			
700	0.52	7.6	1.1
725	0.49	9.7	1.5
750	0.50	11.4	1.4
824	0.49	11.9	2.2
876	0.47	12.0	2.6
928	0.51	12.2	2.8
968	0.49	12.5	3.1
1000	0.50	12.3	4.0

For those literature experiments conducted at pressures <0.7 GPa , externally heated hydrothermal pressure vessels and/or internally heated pressure vessels were employed. Literature experiments done at pressures >0.8 GPa were performed in a piston-cylinder apparatus (Ulmer 1971), similar to the one used in this study. In most cases, experimental aqueous fluid pressures were equal to total pressures. Values of f_{O_2} were controlled by employing the buffer technique of Eugster (1957). Starting materials were similar in composition to the basalt used in the present study. However, although the *P-T* range of some experiments overlapped those of the present work, most pressures and temperatures differed significantly. Accordingly, combining all 65 data sets (analyzed Ca-amphiboles synthesized at specific *P-T* conditions) into one petrogenetic diagram allows the range 0.0–2.2 GPa and 450–1050 °C to be surveyed. Variations in Al_2O_3 and TiO_2 contents of Ca-amphibole in basaltic rocks as a function of temperature and pressure are presented as Figures 8 and 9, respectively. Synthesized Ca-amphiboles are associated with a Ti-rich mineral (ilmenite, rutile, or titanite) and an aluminous phase (garnet, omphacite, or Ca-plagioclase); analyzed amphiboles are thus Ti-saturated and presumably approach Al-saturation as well. However, Ca-amphiboles crystallized from an aluminous basalt protolith (i.e., different from the MORB bulk-rock composition considered in this report) would be expected to exhibit higher contents of Al_2O_3 than the amphiboles produced in the present experiments.

A substantial amount of scatter is evident from these diagrams, possibly reflecting modest differences in bulk-rock compositions used in the various experiments (Table 1). Furthermore, compositions of the Ca-amphiboles must be a complex function of the coexisting phases, especially melt. Nevertheless, the hypothesized chemical variation of Ca-amphibole with changing physical conditions is largely supported. Our experimental and analytical data are not sufficiently numerous to identify *P-T* slope changes in the isopleths, which must occur as a function of phase assemblage; *P-T* inflections are not illustrated where isopleths intersect mineralogic field boundaries because the latter merely indicate appearance-disappearance limits among continuously changing phase proportions.

It is apparent that total Al in Ca-amphibole increases with both pressure and temperature (Fig. 8). Although poorly constrained by the experimental data at high *P* and low *T,* the rate of increase of Al_2O_3 in Ca-amphibole gradually diminishes with rising pressure as greater amounts of garnet join the phase assemblage. Evidently Al is strongly partitioned into garnet relative to amphibole, as is also demonstrated in high-pressure systems containing Al-rich orthopyroxene (MacGregor 1974) and Al-rich talc (Massone 1995). It should be noted in passing that Na_2O isopleths for these synthetic Ca-amphiboles are similar in *P-T* disposition to the Al_2O_3 curves illustrated in Figure 8, reflecting an increase in pargasitic substitution with elevated temperature, and increased glaucophanic substitution with elevated pressure. Because the amphiboles are
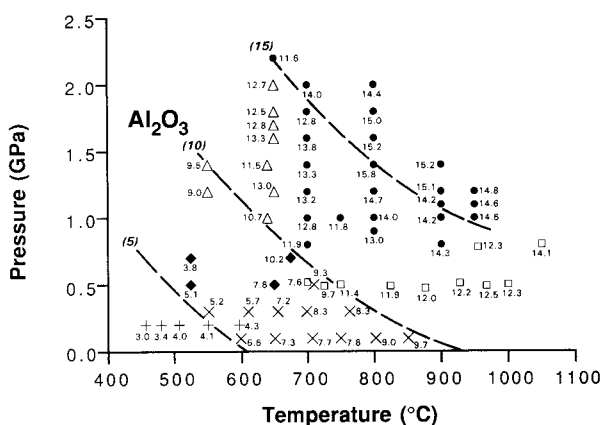
FIGURE 8. Al$_2$O$_3$ contents of synthetic Ca-amphiboles in weight percent as a function of *T* and *P*. Data from: open square = Helz 1973, 1979 ; cross = Liou et al. 1974; X = Spear 1981; filled diamond = Apted and Liou 1983; open triangle = Poli 1993; filled circle = present work. Al$_2$O$_3$ isopleths visually estimated employing moving averages.
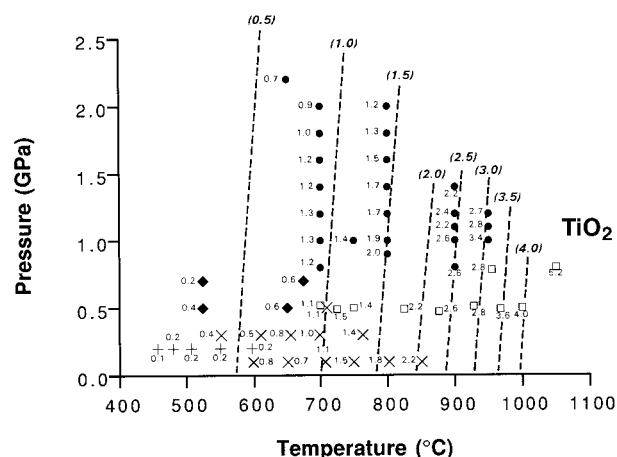

FIGURE 9. TiO$_2$ contents of synthetic Ca-amphiboles in weight percent as a function of *T* and *P*. Data from: open square = Helz 1973, 1979 ; cross = Liou et al. 1974; X = Spear 1981; filled diamond = Apted and Liou 1983; filled circle = present work. TiO$_2$ isopleths visually estimated employing moving averages.

not saturated with respect to Na, their Na contents, like those of Al, are also a sensitive function of variations in bulk-rock composition and phase assemblage.

The Ti content of Ca-amphibole correlates positively with increasing temperature but is nearly independent of pressure (Fig. 9). The Ti content thus represents a relatively quantitative geothermometer at temperatures above 500 °C, where the solubility of Ti in Ca-amphibole becomes substantial (Table 3). The observed slight decrease in TiO$_2$ with increasing pressure over the 2.2 GPa range investigated experimentally suggests that the compliance of the Ca-amphibole octahedral sites accommodating Ti as well as Mg, Fe, and Mn is not greatly diminished at high pressure; perhaps Ti also resides in M1+M3 rather than being confined exclusively to M2 as initially supposed.

The combined Al$_2$O$_3$ and TiO$_2$ isopleths, shown in the *P-T* diagram of Figure 10, constitute a semiquantitative Ca-amphibole thermobarometer for metabasaltic rocks. It seems to be especially applicable at crustal pressures (i.e., up to ~1.2 GPa) and subsolidus temperatures, where the angles of intersection between the Al$_2$O$_3$and TiO$_2$ isopleths are large.

APPLICATION TO NATURAL PARAGENESES

Amphibolite-facies metabasalts characteristically consist of 3–5 phases in an 8–10 component system. Obviously, such high-variance assemblages are not well-constrained, and differences in extensive properties (e.g., bulk-rock composition) will be reflected in changes in phase chemistry independent of *P* and *T*. Natural occurrences that closely match the experimentally determined phase assemblages can be assigned to a *P-T* field (Figs. 1 and 2). For enhanced accuracy, what is needed is a measure of the intensive properties, e.g., chemical potentials of specific components, such as would proxy for the

state variables at the time of metamorphic recrystallization. Concentrations of constituents in Ca-amphiboles offer an approximate solution to this problem. Assuming that the experimentally calibrated Ca-amphibole is saturated with Ti and that the concentration of this component in the amphibole is nearly independent of other chemical parameters (= ideal solid-solution behavior), Figure 9 shows that the TiO$_2$ contents of naturally occurring, homogeneous Ca-amphiboles provide petrologists with a useful geothermometer. Moreover, provided host metabasalts are MORB-like in composition, the Al$_2$O$_3$ contents of Ca-amphiboles (Fig. 8) can serve as *P-T* indicators. The influences of Mg/Fe and f_{O_2} on Ca-amphibole chemistry were not assessed because these parameters were held constant in the experiments. Even so, as demonstrat-
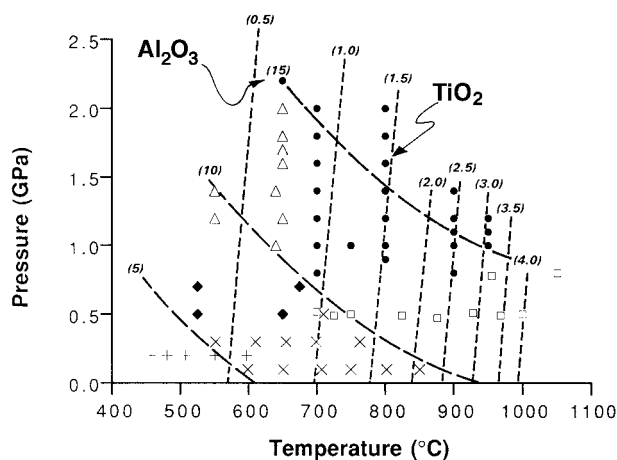

FIGURE 10. Isopleths of Al$_2$O$_3$ and TiO$_2$ in weight percent from Figures 8 and 9.

TABLE 4. Performance of semiquantitative thermobarometer on analyzed Ca-amphiboles from various parageneses

Occurrence	Reference	Original P-T estimates		New hornblende isopleths	
		Avg. T, °C	Avg. P, GPa	Avg. T, °C	Avg. P, GPa*
Sanbagawa Belt, Central Shikoku:	Ernst (1972)				
zone III		400	0.7	560	1.6 (5)
zone I–II boundary		325	0.6	430	0.6 (6)
Gruppo di Voltri, W Liguria:	Ernst (1976)				
hornblendes		440	1.0	480	1.4 (10)
actinolites		300–375	0.2–0.5	365	0.4 (11)
Central Mountain Range, E Taiwan:	Liou et al. (1981)				
amphibolites		670–710	0.5	680	1.1 (12)
greenschists		350–475	0.5	375	0.3 (10)
Archean Basement, NE China:	Ernst (1988)				
high-grade amphibolites		700 ± 50	0.5–0.7	635	0.7
lower grade greenschists		400 ± 50	0.1–0.3	365	0.2 (6)
Central Klamaths, N California:	Ernst et al. (1991),				
relict igneous	Hacker et al. (1992)	~900	0.2–0.3	890	0.7 (8)
metamorphic inner aureole		550	0.3	620	1.3 (1)
metamorphic outer aureole		350	0.3	400	1.0 (1)
White-Inyo Range, E California:	Ernst (1997)				
relict igneous		~875	0.3	880	0.4 (2)
hornblendes		550 ± 50	0.3	525	1.1 (4)
actinolites		~350	0.3	350	0.2 (4)

* ( ) = number of rocks from which naturally occurring clinoamphiboles were analyzed.

ed by the data of Table 1, the bulk compositions of basaltic rocks employed as starting materials for the 65 sets of experiments show considerable variation without invalidating the phase diagram, and isopleths of Figures 8 and 9. The normative mineralogy of the phase-equilibrium starting materials show the following ranges: Quartz 0.0–1.1; Albite 16.7–31.5; Anorthite 18.9–31.8; Diopside 14.9–27.8; Hypersthene 0.0–26.1; and Olivine 0.0–13.7. None of the bulk-rock compositions investigated were Nepheline normative.

Application of the new Ca-amphibole thermobarometer to natural assemblages for which the attendant physical conditions are reasonably well known allows for an assessment of its general utility. Such a test of the thermobarometer was performed utilizing electron-microprobe data for 86 Ca-amphiboles from metabasaltic rocks studied by the first author. These analyzed Ca-amphiboles come from a variety of plate-tectonic settings and P-T regimes: occurrences include eclogite-blueschist-greenschist assemblages from Shikoku and the Ligurian Alps; an amphibolitic continental margin island arc, eastern Taiwan; an Archean basement terrane, northeastern China; an oceanic island arc, northern California; and contact-metamorphosed mafic dikes transecting an Andean-type margin, eastern California. Putative conditions of crystallization are listed in Table 4, according to (1) prior estimates based on phase equilibria and geologic/tectonic constraints, and (2) the new semiquantitative Ca-amphibole thermobarometer. Compared with the earlier P-T estimates, a broad scatter in Al_2O_3- and TiO_2-isopleth-derived conditions for the higher grade Ca-amphibole-bearing metabasalts is evident, with computed pressures systematically high. In contrast, the lower grade, actinolitic parageneses yield more reasonable temperatures and pressures of metamorphism, sensibly identical to those

published previously. Part of this discrepancy may reflect errors in the original P-T estimates.

Temperatures for the low-grade rocks derived from the Ca-amphibole Al_2O_3 and TiO_2 isopleths show the best agreement with previous estimates. This agreement might reflect sluggish reaction rates that inhibited re-equilibration (including exsolution of Ti-bearing phases) of the amphibole on cooling. On the other hand, amphibolite- and granulite-facies Ca-amphiboles probably had sufficient time at high temperatures for titanite, rutile, and/or ilmenite to exsolve, resulting in a substantially lower apparent temperature of amphibole formation in some cases. We note in passing that hornblendes from high-grade metabasalts tend to contain abundant exsolved Ti±Fe inclusions, whereas actinolites from more feebly recrystallized mafic rocks generally exhibit fewer inclusions. In this regard, Mäder et al. (1994) demonstrated that, for Kapuskasing high-grade gneisses, intermediate Fe-Mg-Ca amphibole solid solutions tended to re-equilibrate, yielding somewhat lower calculated amphibole-garnet temperatures compared with biotite-garnet and clinopyroxene-garnet pairs. In contrast to the behavior of Ti, structurally bound Al appears not to have re-equilibrated appreciably during cooling and annealing. For this reason, high-grade Ca-amphiboles exhibit low Ti contents for a given complement of Al, such that the indicated apparent pressures of recrystallization are displaced to unrealistically high values. This kinetic phenomenon represents a serious complication, prohibiting the application of the Ca-amphibole geothermometer to slowly cooled natural rocks unless a correction is made for the exsolved Ti-bearing phase(s). Broad-beam EMPA might be effective in correcting for this phenomenon.

Taking into account these provisos, newly presented and previous experiments demonstrate that, for metabas-

altic assemblages that contain coexisting Al-rich and Ti-rich phases, and closely approached chemical equilibrium under crustal or uppermost mantle conditions, Al_2O_3 and TiO_2 contents of natural Ca-amphiboles can be utilized to estimate semiquantitatively the attendant *P* and *T*.

ACKNOWLEDGMENTS

REFERENCES CITED

Aldridge, L.P., Tse, J.S., Bancroft, G.M., Goldman, D.S., and Rossman, G.R. (1982) The identification of Fe^{2+} in the M4 site of calcic amphiboles: discussion. American Mineralogist, 67, 335–342.

Anderson, J.L. and Smith, D.R. (1995) The effects of temperature and f_{O_2} on the Al-in-hornblende barometer. American Mineralogist, 80, 549–559.

Apted, M.J. and Liou, J.G. (1983) Phase relations among greenschist, epidote-amphibolite, and amphibolite in a basaltic system. American Journal of Science, 283A, 328–353.

Blundy, J.D. and Holland, T.J.B. (1990) Calcic amphibole equilibria and a new amphibole-plagioclase geothermometer. Contributions to Mineralogy and Petrology, 104, 208–224.

Bohlen, S.R. (1984) Equilibria for precise pressure calibration and a frictionless furnace assembly for the piston-cylinder apparatus. Neues Jahrbuch für Mineralogie, 9, 404–412.

Bohlen, S.R. and Boettcher, A.L. (1982) The quartz = coesite transformation: a precise determination and the effects of other components. Journal of Geophysical Research, 87, 7073–7078.

Bohlen, S.R., Essene, E.J., and Boettcher, A.L. (1980) Reinvestigation and application of olivine-quartz-orthopyroxene barometry. Earth and Planetary Science Letters, 47, 1–10.

Deer, W.A., Howie, R.A., and Zussman, J. (1963) Rock-forming Minerals, Chain Silicates. Vol. 2, Wiley, New York, 379 p.

Engel, A.E.J. and Engel, C.E. (1962) Hornblendes formed during progressive metamorphism of amphibolites, northwest Adirondack Mountains, New York. Geological Society of America Bulletin, 73, 1499–1515.

Ernst, W.G. (1972a) Ca-amphibole paragenesis in the Shirataki District, central Shikoku, Japan. Geological Society of America Memoir 135, 73–94.

———(1972b) CO_2-poor composition of the fluid attending Franciscan and Sanbagawa low-grade metamorphism. Geochimica et Cosmochimica Acta, 36, 497–504.

———(1976) Mineral chemistry of eclogites and related rocks from the Voltri Group, Western Liguria, Italy. Schweizerisches Mineralogisches und Petrographisches Mittelungen, 56, 293–343.

———(1979) Coexisting sodic and calcic amphiboles from relatively high pressure metamorphic belts and the stability of barroisitic amphibole. Mineralogy Magazine, 43, 269–278.

———(1988) Element partitioning and thermobarometry in polymetamorphic Late Archean and Early-Mid Proterozoic rocks from eastern Laoning and southern Jilin provinces, People's Republic of China. American Journal of Science, 288A, 293–340.

———(1997) Metamorphism of mafic dikes from the central White-Inyo Range, eastern California. Contributions to Mineralogy and Petrology, 128, 30–34.

Ernst, W.G., Hacker, B.R., Barton, M.D., and Sen, G. (1991) Igneous petrogenesis of magnesian metavolcanic rocks from the central Klamath Mountains, northern California. Geological Society of America Bulletin, 103, 56–72.

Eugster, H.P. (1957) Heterogeneous reactions involving oxidation and re-

duction at high pressures and temperatures. Journal of Chemical Physics, 26, 1760–1761.

Gilbert, M.C., Helz, R.T., Popp, R.K., and Spear, F.S. (1982) Experimental studies of amphibole stability. In Mineralogical Society of America Reviews in Mineralogy, 9B, 229–353.

Graham, C.M. and Powell, R. (1984) A garnet-hornblende geothermometer: calibration, testing, and application to the Pelona Schist, southern California. Journal of Metamorphic Geology, 2, 13–31.

Green, D.H. and Ringwood, A.E. (1967) An experimental investigation of the gabbro to eclogite transformation and its petrological applications. Geochemica et Cosmochimica Acta, 31, 767–833.

Hacker, B.R., Ernst, W.G., and Barton, M.D. (1992) Metamorphism, geochemistry, and origin of magnesian volcanic rocks, Klamath Mountains, California. Journal of Metamorphic Geology, 10, 55–69.

Hawthorne, F.C. (1981) Crystal chemistry of the amphiboles. In Mineralogical Society of America Reviews in Mineralogy, 9A, 1–102.

Helz, R.T. (1973) Phase relations of basalts in their melting range at P_{H_2O} = 5 kb as a function of oxygen fugacity. Journal of Petrology, 14, 249–302.

———(1979) Alkali exchange between hornblende and melt: a temperature-sensitive reaction. American Mineralogist, 64, 953–965.

Hill, R.E.T. and Boettcher, A.L. (1970) Water in the Earth's mantle: melting curves of basalt-water and basalt-water-carbon dioxide. Science, 167, 980–982.

Holland, T.J.B. (1979) High water activities in the generation of high pressure kyanite eclogites of the Tauren Window, Austria. Journal of Geology, 87, 1–27.

Holland, T.J.B. and Blundy, J. (1994) Non-ideal interactions in calcic amphiboles and their bearing on amphibole-plagioclase thermometry. Contributions to Mineralogy and Petrology, 116, 433–447.

Leake, B.E. (1965) The relationship between composition of calciferous amphibole and grade of metamorphism. In W.S. Pitcher and G.W. Flinn, Eds., Controls of Metamorphism, Wiley, New York, 299–318.

———(1978) Nomenclature of amphiboles. Canadian Mineralogist, 16, 501–520.

Leake, B.E., Woolley, A.R., Arps, C.E.S., Birch, W.D., Gilbert, M.C., Grice, J.D., Hawthorne, F.C., Kato, A., Kisch, H.J., Krivovichev, V.G., Linthout, K., Laird, J., Mandarino, J.A., Maresch, W.V., Nickel, E.H., Rock, N.M.S., Schumacher, J.C., Smith, D.C., Stephenson, N.C.N., Ungaretti, L., Whittaker, E.J.W., and Youzhi, G. (1997) Nomenclature of amphiboles: Report of the Subcommittee on Amphiboles of the International Mineralogical Association, Commission on New Minerals and Mineral Names. American Mineralogist, 82, 1019–1037.

Liou, J.G., Kuniyoshi, S., and Ito, K. (1974) Experimental studies of the phase relations between greenschist and amphibolite in a basaltic system. American Journal of Science, 274, 613–632.

Liou, J.G., Ernst, W.G., and Moore, D.E. (1981) Geology and petrology of some polymetamorphosed amphibolites and associated rocks in northeastern Taiwan. Geological Society of America Bulletin, 92, Part I, 219–224, Part II, 609–748.

Liu, J. (1997) High pressure phase equilibria involving the amphibolite-eclogite transformation. unpublished doctoral dissertation, Stanford University,.

Liu, J. and Bohlen, S.R. (1995) Mixing properties and stability of jadeite-acmite pyroxene in the presence of albite and quartz. Contributions to Mineralogy and Petrology, 119, 433–440.

Liu, J., Bohlen, S.R. and Ernst, W.G. (1996) Stability of hydrous phases in subducting oceanic crust. Earth and Planetary Science Letters, 143, 161–171.

MacGregor, I.D. (1974) The system $MgO-Al_2O_3-SiO_2$: Solubility of Al_2O_3 in enstatite for spinel and garnet peridotite compositions. American Mineralogist, 59, 110–1129.

Mäder, U.K. and Berman, R.G. (1992) Amphibole thermobarometry, a thermodynamic approach. In Current Research, Part E, Geological Survey of Canada Paper 92-1E, 393–400.

Mäder, U.K., Percival, J.A., and Berman, R.G. (1994) Thermobarometry of garnet-clinopyroxene-hornblende granulites from the Kapuskasing structural zone. Canadian Journal of Earth Science, 31, 1134–1145.

Massone, H.J. (1995) Experimental and petrogenetic study of UHPM. In

R.G. Coleman and X. Wang, Eds., Ultrahigh-Pressure Metamorphism. Cambridge Press, New York, 33–95.

Melson, W.G., Vallier, T.L., Wright, T.L., Byerly, G., and Nelen, J. (1976) The geophysics of the Pacific Ocean basin and its margin. American Geophysical Union Geophysics Monograph, 19, 351–367.

Moody, J.B., Meyer, D., and Jenkins, J.E. (1983) Experimental characterization of the greenschist/amphibolite boundary in mafic systems. American Journal of Science, 283, 48–92.

Papike, J.J., Cameron, K.L., and Baldwin, K. (1974) Amphiboles and pyroxenes: characterization of other than quadrilateral components and estimates of ferric iron from microprobe data. Geological Society of America Abstracts with Programs, 6, 1053–1054.

Peacock, S.M. (1990) Fluid processes in subduction zones. Science, 248, 329–337.

———(1992) Blueschist-facies metamorphism, shear heating, and P-T-t paths in subduction shear zones. Journal of Geophysical Research, 97, 17,693–17,707.

Popp, R.K., Virgo, D., and Phillips, M.W. (1995) H deficiency in kaersutitic amphiboles: Experimental verification. American Mineralogist, 80, 1347–1350.

Poli, S. (1993) The amphibolite-eclogite transformation: an experimental study on basalt. American Journal of Science, 293, 1061–1107.

Raase, P. (1974) Al and Ti contents of hornblende, indicators of pressure and temperature of regional metamorphism. Contributions to Mineralogy and Petrology, 45, 231–236.

Robinson, P., Spear, F.S., Schumacher, J.C., Laird, J., Klein, C., Evans, B.W., and Doolan, B.L. (1982) Phase relations of metamorphic amphiboles: natural occurrence and theory. In Mineralogical Society of America Reviews in Mineralogy, 9B, 1–227.

Selverstone, J., Franz, G., Thomas, S., and Getty, S. (1993) Fluid variability in 2 GPa eclogites as an indicator of fluid behavior during subduction. Contributions to Mineralogy and Petrology, 112, 341–357.

Shido, F. and Miyashiro, A. (1959) Hornblendes of basic metamorphic rocks. Journal of the Faculty of Science, University of Tokyo, 12, 85–102.

Sorensen, S.S. and Grossman, J.N. (1993) Accessory minerals and subduction zone metasomatism: a geochemical comparison of two melanges. Chemical Geology, 110, 269–297.

Spear, F.S. (1981) An experimental study of hornblende stability and compositional variability in amphibolite. American Journal of Science, 281, 697–734.

Thompson, A.B. (1992) Water in the Earth's upper mantle. Nature, 358, 295–302.

Thompson, J.B. Jr. (1981) An introduction to the mineralogy and petrology of the biopyriboles. In Mineralogical Society of America Reviews in Mineralogy, 9A, 141–188.

Thompson, J.B. Jr., Laird, J., and Thompson, A.B. (1982) Reactions in amphibolite, greenschist, and blueschist. Journal of Petrology, 23, 1–27.

Ulmer, G.C., Ed. (1971) Research Techniques for High Pressure and High Temperature. Springer-Verlag, New York, 367p.

Wolf, M.B. and Wyllie, P.J. (1993) Garnet growth during amphibolite anatexis: implications of a garnetiferous restite. Journal of Geology, 101, 353–373.

Wones, D.R. and Gilbert, M.C. (1982) Amphiboles in the igneous environment. In Mineralogical Society of America Reviews in Mineralogy, 9B, 355–390.

Wood, B.J. and Virgo, D. (1989) Upper mantle oxidation state; ferric iron contents of lherzolite spinels by ^{57}Fe Mössbauer spectroscopy and resultant oxidation fugacities. Geochimica et Cosmochimica Acta, 53, 1277–1291.

Wood, B.J., Bryndzia, L.T., and Johnson, K.E. (1990) Mantle oxidation state and its relation to tectonic environment and fluid speciation. Science, 248, 337–344.

Appendices start on next page

APPENDIX TABLE 1. EMPA of garnet

Experiment no.	112	103	105	158	107	57	59
T (°C)/P (GPa)	950/1.1	950/1.2	950/1.4	950/1.6	900/1.1	900/1.2	900/1.4
No. of analyses (1σ)	11	40	46	43	10	14	8
SiO$_2$	38.29 (41)	38.43 (41)	38.43 (60)	38.88 (52)	38.21 (42)	38.32 (38)	38.53 (61)
Al$_2$O$_3$	22.03 (36)	21.18 (71)	20.89 (80)	22.25 (53)	20.99 (20)	21.41 (60)	21.29 (63)
TiO$_2$	0.82 (16)	1.07 (33)	1.39 (47)	0.75 (33)	0.80 (15)	1.46 (25)	1.60 (09)
FeO	22.21 (38)	21.58 (34)	21.51 (63)	21.26 (50)	22.46 (29)	23.13 (49)	23.32 (72)
MgO	7.91 (28)	8.24 (27)	8.02 (52)	8.62 (48)	7.07 (31)	6.83 (31)	7.52 (45)
MnO	0.92 (07)	0.65 (16)	0.58 (15)	0.52 (05)	0.63 (05)	0.73 (28)	0.71 (16)
CaO	8.51 (39)	8.57 (47)	8.98 (60)	8.64 (65)	9.39 (29)	9.37 (30)	8.56 (30)
Total	100.70 (105)	99.71 (84)	99.82 (120)	100.92 (100)	99.56 (76)	101.25 (155)	101.52 (97)
Formula proportions of cations based on 12 O atoms							
Si	2.93 (01)	2.95 (03)	2.96 (03)	2.95 (02)	2.96 (01)	2.93 (02)	2.93 (06)
Al	1.99 (02)	1.93 (05)	1.89 (06)	1.98 (04)	1.92 (01)	1.93 (03)	1.92 (05)
Ti	0.05 (01)	0.06 (02)	0.08 (03)	0.05 (02)	0.05 (01)	0.08 (01)	0.09 (01)
Fe	1.42 (02)	1.39 (02)	1.38 (04)	1.35 (02)	1.46 (02)	1.48 (02)	1.49 (04)
Mg	0.90 (03)	0.95 (03)	0.92 (05)	0.97 (05)	0.82 (03)	0.78 (03)	0.85 (05)
Mn	0.06 (00)	0.04 (01)	0.04 (01)	0.03 (05)	0.04 (00)	0.05 (02)	0.05 (01)
Ca	0.70 (03)	0.71 (04)	0.74 (05)	0.70 (05)	0.78 (03)	0.77 (02)	0.70 (03)
Sum	8.04 (01)	8.02 (02)	8.01 (02)	8.02 (02)	8.03 (01)	8.02 (01)	8.02 (03)

APPENDIX TABLE 1—Continued

Experiment no.	131	185	187	190	193	160	95
T (°C)/P (GPa)	700/1.2	700/1.4	700/1.4	700/1.4	700/1.6	700/1.8	700/1.6
No. of analyses (1σ)	3	32	24	34	17	32	15
SiO$_2$	38.55 (58)	38.27 (40)	38.25 (37)	38.12 (39)	38.48 (58)	38.27 (71)	38.51 (49)
Al$_2$O$_3$	20.83 (27)	20.38 (29)	20.02 (38)	20.18 (45)	20.57 (33)	21.33 (38)	20.71 (57)
TiO$_2$	0.88 (08)	1.07 (25)	1.44 (50)	1.25 (56)	0.82 (15)	0.85 (16)	1.19 (22)
FeO	22.16 (82)	22.30 (57)	22.04 (208)	21.19 (85)	23.09 (63)	23.90 (80)	22.64 (132)
MgO	2.36 (27)	3.13 (23)	2.82 (44)	2.59 (25)	2.70 (36)	3.01 (25)	3.16 (34)
MnO	1.99 (68)	1.54 (19)	1.28 (43)	1.76 (34)	1.75 (34)	1.41 (49)	1.75 (48)
CaO	13.86 (39)	12.94 (62)	14.06 (126)	14.65 (66)	13.29 (79)	11.87 (49)	12.28 (68)
Total	100.64 (70)	99.64 (80)	99.92 (57)	99.75 (75)	100.70 (56)	100.62 (119)	100.24 (101)
Formula proportions of cations based on 12 O atoms							
Si	3.01 (03)	3.01 (01)	3.00 (02)	3.00 (02)	3.01 (03)	2.98 (03)	3.01 (03)
Al	1.92 (02)	1.89 (02)	1.86 (02)	1.88 (02)	1.89 (03)	1.96 (02)	1.90 (04)
Ti	0.05 (01)	0.06 (01)	0.08 (03)	0.07 (01)	0.05 (01)	0.05 (01)	0.07 (01)
Fe	1.45 (06)	1.47 (03)	1.44 (15)	1.40 (04)	1.51 (05)	1.56 (05)	1.48 (04)
Mg	0.27 (03)	0.37 (02)	0.33 (05)	0.30 (03)	0.31 (04)	0.35 (03)	0.37 (03)
Mn	0.13 (04)	0.10 (01)	0.09 (03)	0.12 (02)	0.12 (02)	0.09 (03)	0.11 (03)
Ca	1.16 (04)	1.08 (04)	1.19 (11)	1.23 (05)	1.11 (06)	0.99 (04)	1.03 (04)
Sum	7.98 (02)	7.99 (01)	7.98 (02)	8.00 (02)	8.00 (02)	7.99 (02)	7.97 (02)

APPENDIX TABLE 2. EMPA of plagioclase

Experiment no.	55	67	70	133	101	97	131	129
T (°C)/P (GPa)	900/1.0	800/1.0	800/1.2	750/1.0	700/0.8	700/1.0	700/1.2	700/1.2
No. of analyses	8	2	3	3	6	8	3	10
SiO$_2$	54.39	57.06	59.68	58.03	58.85	59.24	61.67	57.75
Al$_2$O$_3$	27.42	27.06	25.92	24.60	23.43	25.57	24.28	25.43
FeO	0.63	0.62	0.62	0.83	1.40	0.57	0.79	0.56
MgO	0.04	0.08	0.12	0.24	0.55	0.15	0.34	0.03
CaO	11.01	9.96	8.67	8.89	9.30	8.00	6.51	8.83
Na$_2$O	4.88	4.18	3.86	5.92	4.55	6.92	7.68	5.75
K$_2$O	0.04	0.00	0.08	0.06	0.14	0.04	0.12	0.08
Total	98.40	98.96	98.95	98.55	98.22	100.47	101.39	98.43
Formula proportions of cations based on 8 O atoms								
Si	2.49	2.57	2.67	2.64	2.68	2.64	2.71	2.61
Al	1.48	1.44	1.37	1.32	1.26	1.34	1.26	1.38
Fe	0.02	0.02	0.02	0.03	0.05	0.02	0.03	0.02
Mg	0.00	0.01	0.01	0.02	0.04	0.01	0.02	0.00
Ca	0.54	0.48	0.42	0.43	0.45	0.38	0.31	0.43
Na	0.43	0.37	0.34	0.52	0.40	0.60	0.66	0.51
K	0.00	0.00	0.01	0.00	0.01	0.00	0.01	0.00
Sum	4.98	4.89	4.82	4.96	4.90	4.99	4.99	4.96

APPENDIX TABLE 1—*Continued*

162a 900/1.6 16	61 900/1.6 14	64 900/1.8 14	99 800/1.0 8	70 800/1.2 20	71 800/1.4 25	73 800/1.6 12	175 800/1.6 12	75 800/1.8 18	133 750/1.0 4
38.98 (43)	38.51 (45)	39.02 (48)	38.47 (45)	37.96 (54)	38.17 (55)	38.14 (33)	38.26 (50)	38.14 (48)	38.03 (62)
22.32 (68)	21.39 (50)	21.02 (97)	21.10 (48)	21.29 (25)	21.39 (48)	21.39 (60)	21.76 (48)	21.73 (34)	19.88 (95)
0.68 (35)	1.72 (22)	1.25 (52)	1.03 (18)	1.24 (13)	1.32 (31)	1.16 (24)	1.08 (54)	1.31 (47)	0.88 (16)
22.17 (99)	23.14 (74)	21.23 (86)	21.35 (57)	22.79 (45)	22.14 (72)	21.61 (80)	22.69 (91)	21.51 (139)	22.41 (83)
8.21 (47)	6.82 (60)	7.50 (43)	3.84 (21)	3.96 (26)	4.51 (49)	5.79 (32)	5.70 (58)	5.53 (107)	2.87 (46)
0.50 (09)	0.53 (21)	0.36 (14)	1.75 (09)	1.60 (26)	0.99 (34)	0.51 (15)	0.57 (21)	0.49 (13)	2.32 (13)
8.23 (65)	9.41 (43)	9.72 (83)	12.78 (78)	11.19 (46)	11.41 (57)	10.59 (39)	10.14 (54)	11.30 (67)	12.50 (184)
101.09 (117)	101.52 (74)	100.11 (80)	100.32 (48)	100.03 (79)	99.91 (70)	99.20 (136)	100.20 (99)	100.02 (84)	98.90 (209)
Formula proportions of cations based on 12 O atoms									
2.96 (02)	2.94 (03)	2.99 (03)	2.96 (01)	2.96 (03)	2.98 (03)	2.96 (03)	2.95 (02)	2.95 (02)	3.02 (02)
1.97 (04)	1.93 (04)	1.90 (07)	1.89 (06)	1.96 (03)	1.94 (03)	1.96 (03)	1.98 (02)	2.00 (03)	1.86 (03)
0.04 (03)	0.09 (03)	0.07 (03)	0.08 (04)	0.07 (01)	0.06 (01)	0.07 (01)	0.07 (03)	0.07 (03)	0.05 (01)
1.46 (06)	1.47 (04)	1.36 (05)	1.42 (13)	1.49 (03)	1.39 (04)	1.49 (03)	1.46 (05)	1.39 (10)	1.49 (07)
0.90 (06)	0.79 (08)	0.85 (04)	0.84 (05)	0.46 (03)	0.45 (02)	0.46 (03)	0.65 (07)	0.65 (12)	0.34 (05)
0.03 (01)	0.03 (02)	0.02 (01)	0.02 (00)	0.11 (02)	0.12 (01)	0.11 (02)	0.04 (02)	0.03 (01)	0.16 (01)
0.65 (06)	0.76 (05)	0.80 (07)	0.81 (11)	0.94 (03)	1.05 (05)	0.94 (03)	0.84 (05)	0.92 (06)	1.06 (13)
8.01 (03)	8.01 (01)	7.99 (01)	8.02 (01)	7.98 (02)	7.99 (02)	7.98 (02)	7.99 (02)	7.99 (02)	7.99 (01)

APPENDIX TABLE 1—*Continued*

188 700/1.6 63	189 700/1.6 18	192 700/1.6 14	184 700/1.8 47	140 650/2.2 7	176 650/2.2 70	177 650/2.2 8	178 650/2.2 8	179 650/2.2 16	181 650/2.2 24
38.25 (53)	38.55 (34)	38.37 (22)	38.00 (49)	37.47 (50)	37.65 (28)	37.87 (22)	37.81 (20)	37.45 (63)	37.71 (32)
20.90 (48)	20.27 (27)	20.61 (37)	20.59 (57)	21.58 (28)	21.65 (27)	21.79 (15)	21.85 (15)	21.52 (23)	21.79 (33)
0.90 (26)	1.14 (23)	1.08 (25)	0.82 (22)	0.78 (16)	0.81 (28)	0.79 (23)	0.84 (07)	0.76 (20)	0.61 (13)
23.66 (91)	21.66 (68)	21.99 (90)	24.08 (132)	26.91 (55)	26.17 (57)	25.87 (11)	25.97 (38)	25.81 (27)	25.82 (94)
3.16 (18)	2.93 (21)	2.78 (08)	3.06 (34)	2.73 (18)	3.06 (27)	3.13 (24)	2.93 (15)	3.00 (15)	3.29 (47)
1.86 (41)	1.50 (24)	1.93 (23)	1.47 (48)	1.66 (07)	1.35 (36)	1.11 (15)	1.21 (14)	1.28 (17)	0.91 (21)
12.18 (64)	14.51 (64)	13.86 (70)	11.84 (68)	10.09 (27)	9.41 (32)	10.11 (26)	10.05 (19)	10.13 (38)	10.05 (39)
100.92 (84)	100.55 (65)	100.62 (72)	99.86 (101)	101.27 (84)	100.14 (64)	100.74 (30)	100.73 (40)	100.01 (70)	100.23 (94)
Formula proportions of cations based on 12 O atoms									
2.98 (03)	3.00 (01)	2.99 (02)	3.00 (03)	2.94 (02)	2.96 (02)	2.96 (01)	2.96 (00)	2.96 (02)	2.96 (02)
1.92 (04)	1.86 (02)	1.90 (03)	1.91 (04)	1.99 (01)	2.00 (01)	2.01 (01)	2.01 (01)	2.00 (02)	2.01 (02)
0.05 (01)	0.07 (01)	0.06 (01)	0.05 (01)	0.05 (01)	0.06 (04)	0.05 (01)	0.05 (00)	0.04 (01)	0.04 (01)
1.55 (06)	1.41 (04)	1.43 (06)	1.58 (04)	1.76 (04)	1.72 (03)	1.69 (01)	1.70 (03)	1.70 (02)	1.71 (07)
0.37 (02)	0.34 (02)	0.32 (01)	0.36 (03)	0.32 (02)	0.35 (02)	0.36 (01)	0.34 (02)	0.35 (02)	0.37 (05)
0.12 (03)	0.10 (02)	0.13 (02)	0.10 (03)	0.11 (00)	0.09 (02)	0.07 (01)	0.08 (01)	0.09 (01)	0.06 (01)
1.02 (06)	1.21 (05)	1.16 (06)	1.01 (04)	0.85 (03)	0.79 (03)	0.85 (02)	0.84 (02)	0.85 (03)	0.84 (03)
8.01 (02)	8.00 (01)	8.00 (01)	8.00 (02)	8.02 (01)	7.99 (02)	8.00 (01)	7.99 (01)	8.00 (01)	8.00 (02)

APPENDIX TABLE 3. EMPA of clinopyroxene

Experiment no. T (°C)/P (GPa) No. of analyses (1σ)	103 950/1.2 10	105 950/1.4 32	158 950/1.6 45	107 900/1.1 6	59 900/1.4 6	61 900/1.6 30	64 900/1.8 34	73 800/1.6 7
SiO₂	47.19 (76)	48.13 (95)	50.43 (79)	46.67 (60)	48.15 (76)	49.47 (125)	51.17 (59)	49.07 (72)
Al₂O₃	7.63 (91)	7.23 (114)	4.61 (118)	7.96 (51)	9.11 (97)	8.82 (145)	5.78 (192)	7.57 (102)
TiO₂	1.12 (28)	0.97 (15)	0.68 (20)	1.10 (11)	0.97 (19)	0.91 (26)	0.59 (19)	0.90 (45)
FeO	10.95 (41)	11.27 (61)	12.66 (73)	10.30 (44)	10.52 (57)	10.43 (86)	11.68 (95)	9.74 (73)
MgO	11.76 (55)	11.18 (75)	9.88 (58)	12.68 (49)	12.62 (106)	10.40 (83)	9.10 (100)	9.43 (73)
MnO	0.23 (04)	0.18 (06)	0.12 (02)	0.17 (02)	0.22 (08)	0.11 (06)	0.09 (03)	0.15 (07)
CaO	18.35 (34)	18.84 (80)	20.10 (44)	20.03 (33)	17.22 (109)	18.01 (62)	19.23 (66)	20.12 (46)
Na₂O	0.83 (04)	1.08 (10)	1.04 (41)	0.79 (03)	1.26 (21)	1.91 (18)	1.78 (54)	1.43 (15)
Total	98.07 (59)	98.87 (68)	99.52 (88)	99.69 (82)	100.07 (91)	100.06 (71)	99.42 (84)	98.40 (65)
Formula proportions of cations based on 6 O atoms								
Si	1.82 (03)	1.84 (02)	1.89 (02)	1.78 (01)	1.81 (02)	1.83 (04)	1.91 (03)	1.88 (03)
Al	0.34 (04)	0.31 (04)	0.21 (05)	0.36 (03)	0.40 (04)	0.39 (07)	0.25 (09)	0.31 (07)
Ti	0.03 (01)	0.03 (00)	0.02 (01)	0.03 (00)	0.03 (01)	0.03 (01)	0.02 (00)	0.02 (01)
Fe	0.63 (02)	0.65 (03)	0.71 (04)	0.59 (02)	0.59 (03)	0.57 (05)	0.65 (06)	0.58 (05)
Mg	0.38 (02)	0.35 (02)	0.31 (02)	0.41 (02)	0.40 (03)	0.33 (03)	0.28 (03)	0.29 (01)
Mn	0.01 (00)	0.01 (01)	0.00 (00)	0.01 (00)	0.01 (01)	0.00 (00)	0.00 (00)	0.00 (00)
Ca	0.76 (01)	0.77 (03)	0.81 (02)	0.82 (01)	0.69 (04)	0.72 (02)	0.77 (03)	0.82 (01)
Na	0.06 (00)	0.08 (01)	0.08 (03)	0.06 (00)	0.09 (02)	0.14 (01)	0.13 (04)	0.10 (02)
Sum	4.02 (00)	4.02 (02)	4.02 (01)	4.04 (00)	4.02 (01)	4.01 (01)	4.01 (01)	4.00 (01)

APPENDIX TABLE 4. EMPA of quenched glass

Experiment no. T (°C)/P (GPa) No. of analyses	116 950/1.0 2	112 950/1.1 3	103 950/1.2 6	105 950/1.4 7	158 950/1.6 5	53 900/0.8 4	55 900/1.0 2	99 900 4
SiO₂	54.13	56.31	57.18	58.72	57.03	58.04	58.43	56.07
Al₂O₃	18.01	18.06	18.37	17.64	14.94	17.24	17.26	17.3
TiO₂	1.13	0.96	0.88	0.62	1.38	0.99	0.69	1.04
MgO	0.94	0.77	0.27	0.5	1.18	0.74	1	0.76
MnO	0.19	0.10	0.05	0.03	0.06	0.14	0.16	0.05
FeO	10.11	5.68	3.23	2.65	4.72	4.9	5.65	7.87
CaO	4.7	5.65	4.74	4.47	5.56	5.76	6.31	5.69
Na₂O	1.31	0.57	0.47	0.66	0.54	0.33	0.77	0.24
K₂O	0.31	0.28	0.25	0.33	03.2	0.23	0.24	0.27
Total	90.81	88.37	85.42	85.62	85.72	88.36	90.48	89.28

APPENDIX TABLE 3—*Continued*

75 800/1.8 27	184 700/1.8 24	183 700/1.8	197 700/2.0 68	176 650/2.2 46	177 650/2.2 14	178 650/2.2 20	179 650/2.2 6	181 650/2.2 25	140 650/2.2 8
50.84 (67)	52.14 (52)	52.29 (43)	51.69 (55)	52.40 (92)	53.41 (94)	52.45 (72)	52.24 (56)	53.61 (77)	52.66 (82)
7.11 (91)	8.18 (124)	8.26 (87)	8.43 (95)	10.18 (95)	9.65 (89)	10.05 (100)	10.29 (75)	11.61 (99)	9.80 (64)
0.69 (34)	0.62 (33)	0.58 (29)	0.52 (24)	0.63 (35)	0.37 (11)	0.84 (58)	0.81 (64)	0.35 (14)	0.34 (05)
10.81 (58)	8.26 (55)	8.07 (46)	9.42 (56)	7.27 (58)	8.66 (98)	8.09 (72)	7.69 (55)	7.38 (70)	7.52 (30)
7.76 (36)	9.28 (65)	9.30 (66)	7.74 (94)	9.18 (65)	6.88 (134)	8.37 (75)	8.10 (95)	6.76 (93)	10.26 (49)
0.07 (02)	0.15 (04)	0.16 (05)	0.09 (04)	0.20 (03)	0.09 (06)	0.10 (03)	0.14 (04)	0.09 (03)	0.23 (02)
19.14 (98)	16.56 (107)	16.38 (61)	18.00 (66)	13.79 (73)	15.19 (89)	14.07 (98)	14.60 (46)	13.42 (72)	14.08 (96)
2.15 (57)	4.38 (49)	4.34 (54)	3.79 (47)	5.33 (41)	5.03 (61)	5.12 (38)	5.09 (22)	6.09 (42)	4.93 (42)
98.57 (57)	99.58 (61)	99.39 (51)	99.67 (77)	98.96 (70)	99.29 (91)	99.09 (52)	98.96 (86)	99.30 (85)	99.81 (105)
Formula proportions of cations based on 6 O atoms									
1.90 (02)	1.93 (02)	1.94 (01)	1.91 (01)	1.94 (03)	1.95 (03)	1.95 (03)	1.88 (03)	1.92 (03)	1.94 (01)
0.29 (06)	0.36 (05)	0.36 (04)	0.37 (04)	0.45 (04)	0.42 (03)	0.41 (04)	0.35 (05)	0.32 (07)	0.43 (03)
0.02 (01)	0.02 (01)	0.02 (01)	0.02 (01)	0.02 (01)	0.01 (00)	0.02 (01)	0.02 (02)	0.02 (01)	0.01 (00)
0.62 (04)	0.46 (03)	0.45 (03)	0.52 (03)	0.40 (03)	0.46 (06)	0.41 (03)	0.57 (05)	0.60 (06)	0.41 (02)
0.25 (01)	0.29 (02)	0.29 (02)	0.24 (03)	0.28 (02)	0.24 (03)	0.32 (02)	0.28 (02)	0.25 (04)	0.32 (02)
0.00 (00)	0.00 (00)	0.01 (01)	0.00 (00)	0.01 (00)	0.00 (00)	0.01 (00)	0.01 (00)	0.00 (00)	0.01 (00)
0.78 (04)	0.66 (05)	0.65 (03)	0.71 (03)	0.55 (03)	0.59 (05)	0.50 (02)	0.72 (02)	0.69 (03)	0.56 (04)
0.14 (04)	0.31 (03)	0.31 (04)	0.27 (03)	0.38 (03)	0.35 (04)	0.38 (05)	0.18 (02)	0.21 (04)	0.35 (03)
4.00 (01)	4.03 (02)	4.02 (01)	4.03 (01)	4.01 (01)	4.01 (01)	4.01 (02)	4.01 (01)	4.01 (01)	4.02 (01)

APPENDIX TABLE 4—*Continued*

57 900 2	59 900/1.4 5	162 900/1.4 3	61 900/1.6 4	63 900/1.8 2	149 800/2.2 8	122 800/2.4 2	146 800/2.0 5	75 800/1.8 3	144 750/2.2 1
60.81	65.14	56.03	64.02	60.64	67.04	66.6	66.19	64.07	69.04
17.06	17.12	13.06	16.09	15.3	13.41	14.14	13.84	14.12	12.51
0.63	0.62	0.79	0.47	0.68	0.27	0.26	0.24	0.21	0.17
0.48	0.69	1.28	0.43	0.31	0.38	0.74	0.23	0.11	0.12
0.04	0.03	0.09	0.01	0.01	0.03	0.06	0.01	0.02	0
3.37	2.9	6.7	1.99	1.58	1.39	1.55	0.88	0.61	0.73
4.53	2.78	5.71	2.3	3.01	1.85	2.49	1.41	1.58	1.57
0.48	0.72	0.94	1.02	1.7	1.37	3.19	2.25	4.27	0.35
0.27	0.40	0.26	0.43	0.47	0.82	0.66	1.16	0.43	0.94
87.67	90.41	84.85	86.76	83.7	86.56	89.65	86.23	85.41	85.43